

UNIVERSITÀ DEGLI STUDI DI GENOVA
Scuola Politecnica
DICCA

UNIVERSITÉ PIERRE ET MARIE CURIE
Institut Jean Le Rond d'Alembert
Paris



Stability analysis of liquid bridges

Author:
Andrea TRIPODI

Supervisor:
Prof. Alessandro BOTTARO
Dr. Jerome HOEPFFNER

Academic year 2013/2014

Abstract

Drop formation is a very interesting and common phenomenon that can be seen in a wide range of occurrences, both natural and man-made, from rain drops to ink-jet printers and spray atomizers. It is also a topic that fascinated scientists for centuries and the mathematical description pioneered by Young and Laplace opened the door to their systematic study. Drop formation starts with an elongated filament, or liquid bridge, which connects the drop to the body of liquid that subsequently necks by capillary action and breaks into droplets.

The main goal of this thesis is to develop a tool for investigating the stability of the equilibrium state of liquid bridges, which is the last connection between the drop and the body of liquid. For this aim, bifurcation theory and linear stability analysis have been used by developing a MATLAB code, and adopting numerical tool, like pseudo-arclength continuation and the Newton-Raphson method.

After some historical considerations, the one-dimensional model by Eggers and Dupont is presented. A brief description of bifurcation and linear stability analysis is provided with some examples linked to our topic. On this basis, details and issues on the numerical procedure and methods in use are accurately explained and the validation of our tool is presented. Finally, the results of the stability analysis are shown on the influence of characteristic dimensionless parameters on breakup.

Sommario

La formazione di gocce è un fenomeno comune e molto interessante, visibile ogni giorno in una grande varietà di eventi, sia naturali che artificiali. Molte applicazioni ingegneristiche utilizzano questo meccanismo per arrivare a scopi differenti; per averne un'idea, basti solo pensare alla verniciatura delle carrozzerie delle automobili, agli iniettori di combustibile per motori a combustione interna o alle stampanti a getto d'inchiostro. Inoltre, nella nostra vita di tutti i giorni assistiamo continuamente a questa manifestazione; chiunque di noi è familiare con la noiosa formazione delle goccioline dal rubinetto o lo spray di profumi e deodoranti solo per citarne alcuni.

Ognuna di queste applicazioni ha come scopo la formazione di gocce di dimensioni controllate a seconda del tipo di utilizzo. Esistono molti modi per produrle ma, essenzialmente, da una riserva di liquido si forma un filamento allungato di liquido (o "ponte liquido"); questo successivamente si assottiglia formando una strizione e, infine, si rompe dando vita alla goccia.

Lo scopo principale di questa tesi è quello di sviluppare uno strumento per analizzare la stabilità dei punti di equilibrio del ponte liquido, ultima connessione tra la goccia e il resto del filamento. A tal scopo è stato sviluppato un codice in MATLAB che si basa su strumenti come la teoria della biforcazione e quella della stabilità lineare, assieme a metodi di continuazione della soluzione e di calcolo degli zeri.

Nella prima parte di questa tesi, dopo un'introduzione al problema e alla storia delle ricerche scientifiche, viene presentato il modello semplificato utilizzato in questo studio. Successivamente vengono descritti in dettaglio gli strumenti matematici utilizzati e le procedure numeriche. Infine, vengono mostrati i risultati ottenuti e i possibili sviluppi futuri. Nel dettaglio, la tesi si suddivide in sette sezioni, di seguito descritte in modo esaustivo.

La prima sezione è puramente introduttiva; dopo un primo inquadramento del fenomeno della formazione delle gocce, viene fatta una panoramica degli sviluppi delle ricerche su questo argomento nel corso degli anni.

La seconda sezione riguarda il modello fisico-matematico utilizzato per descrivere il ponte liquido. Si tratta di un modello mono-dimensionale noto in letteratura e proposto da Eggers e Dupont nel 1994, di cui viene presentata in modo riassuntivo la sua derivazione partendo dalle equazioni di Navier-Stokes.

Nella terza sezione, si descrive la teoria della biforcazione, il suo utilizzo e le maggiori considerazioni che si possono trarre da essa. Viene inoltre trattato l'utilizzo del diagramma di biforcazione e analizzati i principali punti d'interesse che si possono incontrare in questo studio.

La quarta sezione è dedicata alla teoria della stabilità lineare; viene presentato il procedimento generale e alcuni risultati generici. Oltre a ciò, viene fatta un'attenta analisi del diagramma di stabilità del ponte liquido.

La quinta sezione raggruppa tutti i metodi numerici utilizzati per sviluppare il codice di calcolo: di ognuno si descrive la teoria, l'implementazione numerica e si analizzano i limiti e i benefici che possono dare.

Infine, la sesta e settima sezione sono dedicate rispettivamente ai risultati e alle conclusioni e sviluppi futuri.

Contents

1	Introduction	7
1.1	History	9
2	The liquid bridge	17
2.1	Geometrical configuration	17
2.2	The mathematical formulation	19
3	Bifurcation theory	22
3.1	Stationary solution	22
3.2	Bifurcation diagram	23
3.3	Singular point	25
4	Linear stability analysis	28
4.1	The linearisation	29
4.2	The stability analysis	31
4.3	Stability diagram	32
5	Numerical procedure	35
5.1	The NewtonRaphson method	35
5.2	Continuation of solution - Pseudo-arclength continuation	36
5.3	Bifurcation point and branch switching	37
5.4	Step-size control	38
5.5	Numerical differentiation	39
5.6	Code validation	40
5.7	Code for integration in time	43
6	Simulation results	45
6.1	Influence of Weber number on stability limit	45
6.2	Influence of Ohnesorge number (Oh)	49
6.3	Comparison with quasi-static simulations	52

<i>CONTENTS</i>	6
7 Conclusions and future work	57
Ringraziamenti	58

1 Introduction

From rain drops to very tiny, pico-litre sized drops produced in an ink-jet printer, drop formation is seen in a wide range of occurrences, both natural and man-made. This common physical occurrence is driven by surface tension of the liquid, which tends to minimize the interface area between immiscible fluids.

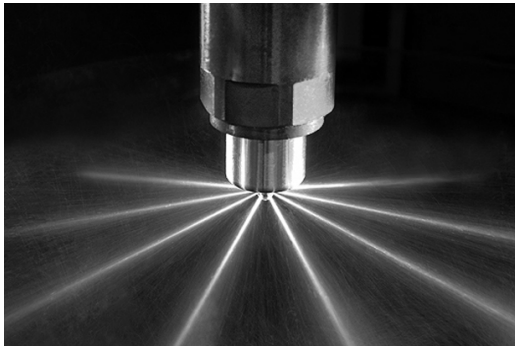
A variety of modern engineering applications employ drop formation to achieve different purposes. Just to give an idea, we can mention: spray-painting (figure 1.1(e)), liquid fuel atomizer for internal combustion engine (figure 1.1(a)), ink-jet printing (figure 1.1(f)), agricultural irrigation, medical diagnostics, manufacturing.

However, droplets formation is also present in our everyday environment in kitchens, showers, pharmaceutical sprays and cosmetics, and are also used for our entertainment, and for our security. Everyone is familiar with the annoying formations of droplets from faucet (figure 1.1(d)), the spray of a perfume bottle (figure 1.1(b)), fire extinguishers or dropper (figure 1.1(c)).

All of these processes have as ultimate goal to produce drops of controlled volumes and compositions depending upon the final requirement. There are several methods to produce drops from nozzles. In all of these methods, essentially, an elongating liquid filament or a liquid bridge is formed connecting two "blobs" or reservoirs of the liquid. This filament subsequently thins or necks by capillary action or by externally applied strains, and breaks forming individual drops.

In this thesis the focus will be on the *breakup* of liquid bridge which is the last thin connection between the drop and the macroscopic body of liquid. In particular, we will investigate the stability of the equilibrium state since it can be a guide to the dynamics of the system: looking at steady states and bifurcations can tell us more about the dynamics of a liquid bridge's evolution and the phenomenon of the creation of drop.

On the analytical side, linear stability analysis is a basic but precious tool. Anyway, non linear effects are important - if not dominant - in the dynamics of the process. Numerically, solving the Navier-Stokes equation (NSE) for these



(a)



(b)



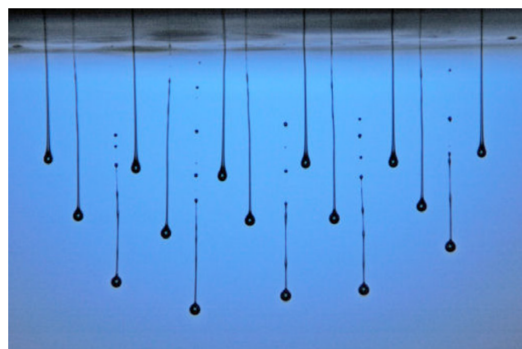
(c)



(d)



(e)



(f)

Figure 1.1: Example of applications employing drop formation: (a) fuel injector, (b) spray of a perfume bottle, (c) dropper, (d) falling droplet from a faucet, (e) spray painting, (f) drops from a bank of ink-jet nozzles

problems remains a challenging task in term of computational effort, due to the high resolution needed near break-up. For this reason, reduced-order models have been developed in the past and are available in the literature. In this thesis we will employ a one-dimensional model, based on a lowest-order expansion in Taylor series of the Navier-Stokes equations, to model the liquid bridge. We will also employ bifurcation methods and linear stability theory to investigate the equilibria of liquid bridges.

Apart from its own interest on ground for natural capillary systems, the liquid bridge configuration offers some unique characteristics that makes it interesting for fluid physics research under microgravity. On the one side, the liquid bridge is the simplest mechanical model of the floating zone technique of crystal growth, a key process in material sciences for purification in a crucible-free configuration. On the other side, a particular instance of liquid bridges (the cylindrical shape) is one of the simpler free interfaces one can establish in space; the other (simplest) cases, the flat surface and the sphere are much more difficult to handle. Consequently, the liquid bridge configuration has been extensively used to study a number of difficult problems, like Marangoni convection.

For the importance on basic research and the wide range of applications, droplet formation is a topic that fascinated scientists for centuries. We present here some history about scientific research on jets and droplets. Most of the information come from [6, 7, 9, 18].

1.1 History

Flows involving free surfaces lend themselves to observation, and thus have been scrutinized for hundreds of years. The earliest theoretical work was concerned almost exclusively with the equilibrium shapes of fluid bodies, and with the stability of the motion around those shapes. Experimentalists, always being confronted with physical reality, were much less able to ignore the strongly non-linear nature of hydrodynamics. Thus many of the non-linear phenomena, that are the focus of attention today, had already been reported 170 years ago. However, with no

theory in place to put these observations into perspective, non-linear phenomena took the back seat to other issues, and were soon forgotten.

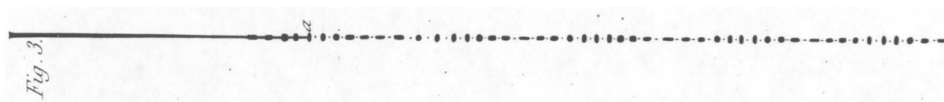


Figure 1.2: The breakup of liquid jet from Savart's original paper [24]. It clearly shows the succession of main and satellite drops as well as drop pscillations

The first mention of drop formation in the scientific literature is in a book by Mariotte (1686) on the motion of fluids. He notes that a stream of water flowing from a hole in the bottom of a container decays into drops. Like many authors after him, he assumed that gravity, or other external forces, are responsible for the process.

Mariotte argued that a falling jet acquires a speed corresponding to free fall $v = \pi\sqrt{2gx}$ at a distance x from the nozzle. Then, mass conservation gives the relation for the radius h of the jet

$$h = \left[\frac{Q}{\pi\sqrt{2gx}} \right]^{1/2},$$

where Q is the flow rate. The ideas of Mariotte suggest that cohesive forces provide a certain tensile strength σ of water, which has to be overcome by gravity for the jet to break.

One hundred years later, a great contribution to the resolution of this problem was made by Laplace [4] and Young [29], who published their celebrated work, demonstrating the crucial role of the mean curvature, made up of contributions from both the axial and the radial curvature. The subtle point which leads to the fallacy of earlier authors is that surface tension can act in two different ways: while for a hanging drop it indeed acts like an elastic membrane, once a cylindrical shape is reached the radial curvature drives the breakup! Namely, the system is driven towards a state having a smaller surface area, and thus towards a

smaller jet radius, which eventually goes to zero. Thus paradoxically, the greater the cohesion between the particles (and thus the surface tension γ), the faster breakup occurs.

The basis for a more thorough understanding of drop formation was laid in 1833 by Savart [24], who very carefully investigated the decay of fluid jets. He was the first to recognize that the breakup of liquid jets is governed by laws independent of the circumstances under which the jet is produced, breakup always occurs independently of the direction of gravity, the type of fluid, or the jet velocity and radius, and thus must be an intrinsic property of the fluid motion.

Without photography at Savart's disposal, experimental observation of drop breakup is very difficult, since the timescale on which it takes place is very short. Yet, Savart was able to extract a remarkably accurate and complete picture of the actual breakup process using his naked eye alone. To this end, he used a black belt, interrupted by narrow white stripes, which moved in a direction parallel to the jet. This effectively permitted a stroboscopic observation of the jet. To confirm beyond doubt the fact that the jet breaks up into drops and thus becomes discontinuous, Savart moved a "*slender object*" swiftly across the jet, and found that it stayed dry most of the time.

Savart's insight into the dynamics of breakup is best summarized by figure 1.2 taken from his paper [24]. To the left one sees the continuous jet as it leaves the nozzle. Perturbations grow on the jet, until it breaks up into drops, at a point labelled *a*. Near *a* an elongated neck has formed between two bulges which later become drops. After breakup, in between two such drops, a much smaller "*satellite*" drop is always visible. Owing to perturbations received when they were formed, the drops continue to oscillate around a spherical shape. Only the very last moments leading to drop formation are not quite resolved in figure 1.2.

The crucial role of surface tension was recognized in 1849 by Plateau [21], who confined himself mostly to the study of equilibrium shapes and whether a given perturbation imposed on a fluid cylinder would grow or not. Namely, any perturbation that leads to a reduction of surface area is favoured by surface tension, and will thus grow. This makes all sinusoidal perturbations with wavelength

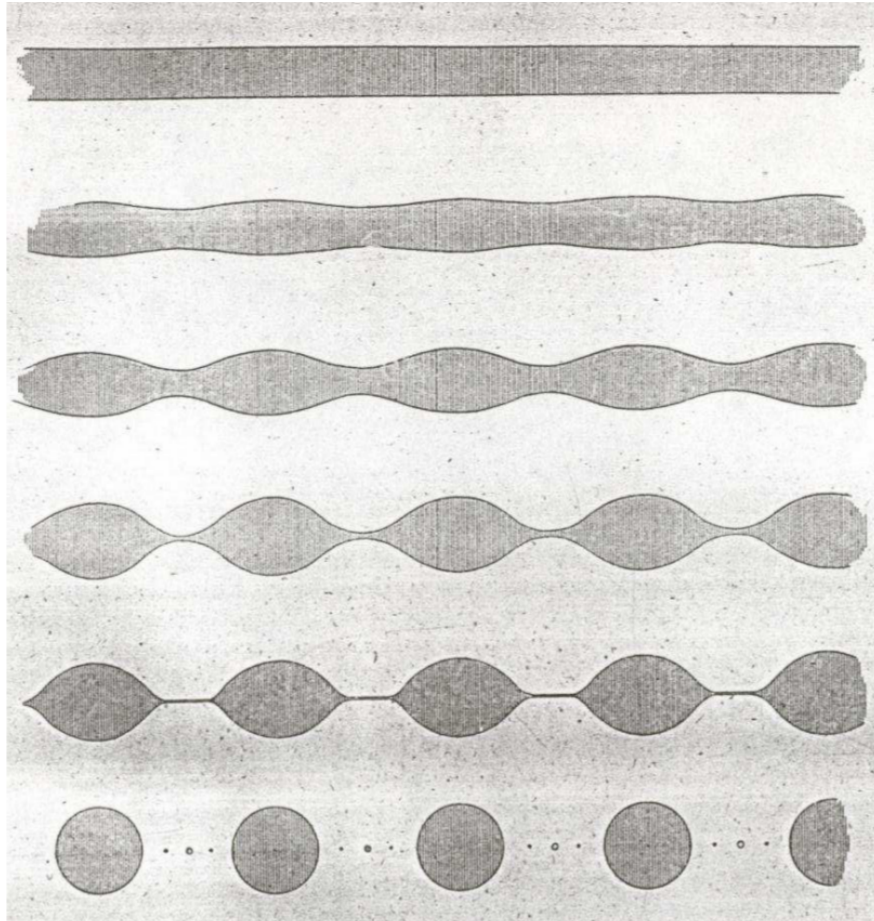


Figure 1.3: Breakup of liquid column of oil suspended in a mixture of alcohol and water from Plateau [21]

longer than 2π unstable.

A little earlier (1843), Plateau had developed his own experimental technique to study drop breakup [20], by suspending a liquid bridge in another liquid of the same density in a so-called "*Plateau tank*", thus eliminating the effects of gravity. Yet this research was focused on predicting whether a particular configuration would be stable or not (figure 1.3).

Following up on Plateaus insight, Rayleigh [22] realized that to understand the breakup process the flow dynamics has to be taken into account. He noticed

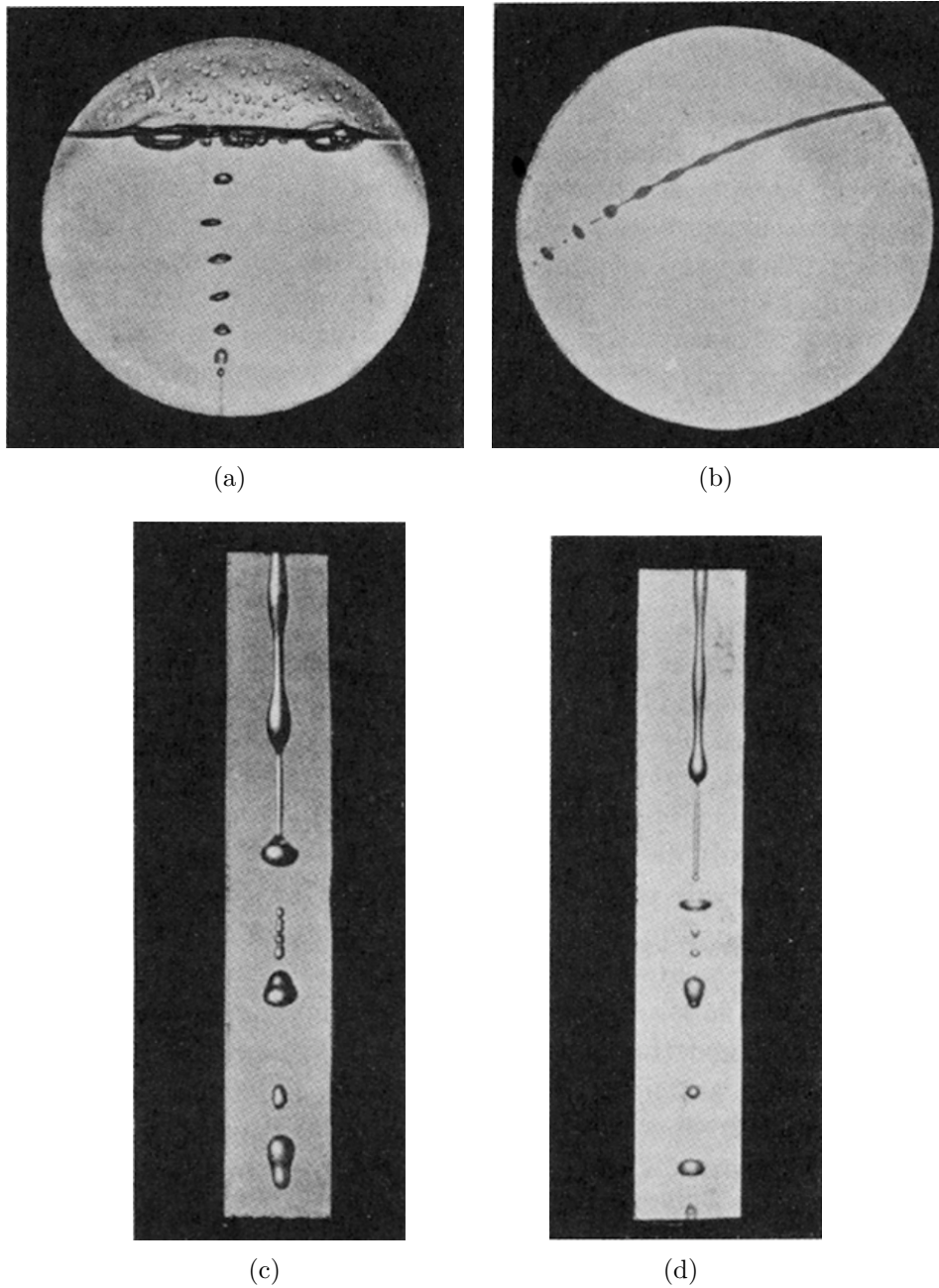


Figure 1.4: Plate I of Rayleigh's "some applications of photography" (1891) showing the destabilization of a jet of air into water (*a*) and of a water jet in air (*b*). Rayleigh notes that the air jet destabilizes faster than the water jet. Details of the breakup process and the recoil of initially straight "ligaments" between the drops, sometimes breaking themselves before they have recoiled, we shown in figure (*c*) and (*d*).

that surface tension has to work against inertia, which opposes fluid motion over long distances. By considering small sinusoidal perturbations on a fluid cylinder of radius r , Rayleigh found that there is an optimal wavelength, $\lambda_R \approx 9r$, at which perturbations grow fastest, and which sets the typical size of drops. Analysing data Savart had obtained almost 50 years earlier, Rayleigh was able to confirm his theory to within 3%. Accordingly, the time scale τ on which perturbations grow and eventually break the jet is given by a balance of surface tension and inertia, and thus

$$\tau = \sqrt{\frac{r^3 \rho}{\gamma}}$$

where ρ is the density, r the radius of the thread and γ the coefficient of surface tension of the fluid. This tells us two important things: substituting the values for the physical properties of water and $r = 1$ mm, one finds that τ is 4 ms, meaning that the last stages of pinching happen very fast, far below the time resolution of the eye. Secondly, as pinching progresses and r gets smaller, the time scale becomes shorter and pinching precipitates to form a drop in a *finite time*.

Rayleigh's linear stability calculation of a fluid cylinder only permits to describe the initial growth of instabilities as they initiate near the nozzle. It certainly fails to describe the details of drop breakup leading to, among others, the formation of satellite drops. Linear stability analysis is however quite a good predictor of important quantities like the continuous length of the jet. Of course, as soon as the perturbations are no longer small, non-linear effects become important, and eventually dominate close to breakup. The features of this non-linear dynamics were revealed in increasingly sophisticated experiments.

Rayleigh was well aware of the intricacies of the last stages of breakup, and published some experimental pictures himself (Rayleigh (1891)). Unfortunately, these pictures were produced by a single short spark, so they only transmit a rough idea of the dynamics of the process. However, it is again clear that satellite drops, or entire sequences of them, are produced by elongated necks between two main drops. Clearly, what is needed for a more complete understanding is a sequence

of photographs showing how one evolves into the other.

We have to wait till the work of Lenard [14] in 1887 who records a sequence showing the dynamics close to breakup, leading to the separation of drop. It shows for the first time the origin of the satellite drop (figure 1.5): first the neck breaks close to the main drop and then it also pinches on the side toward the nozzle just before it can snap back. Thus, the sequence demonstrates that the satellite drop comes from an elongated neck, the form of which is imposed by the asymmetry of the profile close to the pinch point: on one side it is very flat, on the other it merges into the spherical shape of a drop.

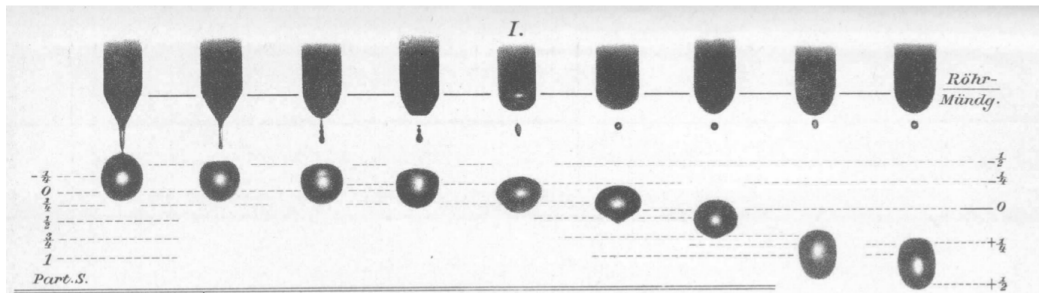


Figure 1.5: A sequence of pictures of a drop of water falling from a pipette from the experiment of Lenard [14]. For the first time, the sequence of events leading to satellite drop formation can be appreciated.

More recently, experimental techniques have also become available with sufficient resolution in space and time to look at the immediate vicinity of the point of breakup. Notable examples include the jet experiments in 1970 of Rutland and Jameson as well as those of Goedde and Yuen for water jets and in 1996 of Kowalewski for jets of high-viscosity fluids. A momentous paper in 1990 by Peregrine, Shoker, and Symon not only helped to crystallize some of the theoretical ideas, but also contained the first high-resolution pictures of water falling from a tap.

By comparison, the development of computer codes that would permit the calculation of free-surface flows from first principles has been slow. Owing to the difficulties involved in implementing both moving boundaries and surface tension,

resolution has not been possible anywhere near the experimentally attainable limit, even with present-day computers. Only gradually did the theoretical tools evolve that allowed for an analytical description of the non-linear dynamics close to breakup. The first was developed in the theory of waves and often goes by the name of "*lubrication theory*" or "*the shallow-water approximation*" by Peregrine in 1972. It captures non-linear effects in the limit of small depths compared with a typical wavelength. During the 1970s, lubrication approximations were developed for the corresponding axisymmetric problem, to study drop formation in ink-jet printers. This is of particular relevance since a jet does not break up uniformly, as predicted by linear theory, but rather into main drops and much smaller "satellite" drops. The satellite drops fundamentally limit the print quality attainable with this technology, as drops of different sizes are deflected differently by an electric field which should direct the stream of droplets to a given position on the paper.

Thus a fully non-linear theory is needed to understand and to control the formation of satellite. The first dynamical equation, based on lubrication ideas, was introduced in 1974 by Lee for the inviscid case. His non-linear simulations indeed showed the formation of satellite drops. But it took two decades until systematic approximations of the Navier-Stokes equation were found that included viscosity (Bechtel, Forest and Lin; Eggers and Dupont [8]).

With the beginning of the space era in the late 1960s arose the need to know better about capillary systems and the opportunity to experiment in a much better environment with them than on the ground. Research in low-gravity fluid physics has gone hands-in-hands with space exploration due to the need to solve new technological problems like liquid gauging and sloshing in spacecraft tanks, and to better understand old technological problems like wetting and spreading, breaking of drops, jets and liquid bridges, etc. It started in Europe with the space era in the sixties, but only reached critical size in the seventies after the Call-for-Ideas for the Spacelab experiments (ESRO-1974), that matured around ESAs Fluid Physics Module (FPM) flown in the first Spacelab payload in 1983.

2 The liquid bridge

A single-connected blob of liquid is called drop if it is completely surrounded by another fluid (isolated drop) or in touch just one solid surface in a single-connected solid-liquid interface (captive drop). If the liquid touches more solid boundaries (unconnected solid-liquid interface) it is called a liquid bridge (see figure 2.1), the common case being a liquid bridge spanning between two solid surface. If the liquid mass is issuing through a hole in a solid, it is called jet. Of course, these simple geometries might be combined and thus compound geometries, like a drop inside a drop or a jet inside a jet might appear.

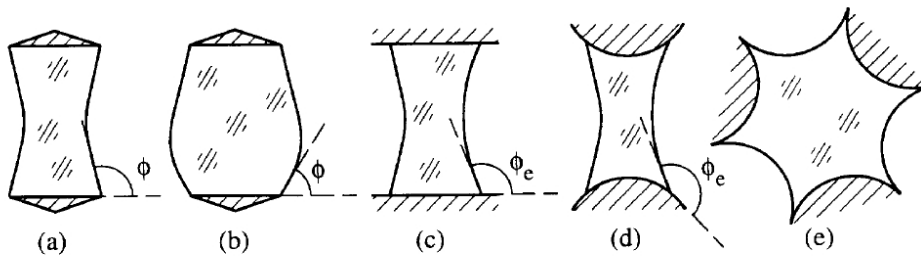


Figure 2.1: Various configurations of liquid bridges between solid supports

In this work, we consider only the special case of a liquid bridge. Liquid bridges occur in a variety of physical and technological situations and a great deal of theoretical and experimental work has been done to determine axisymmetric equilibria for various disk configurations, bridge slenderness and rotations. There have also been numerous investigations of the dynamics of axisymmetric liquid bridges subject to excitations and some research has been performed also on non-axisymmetric bridge stability

2.1 Geometrical configuration

In the simplest configuration, a liquid bridge consists of a mass of liquid held by surface tension forces between two parallel solid disks, as sketched in figure 2.2.

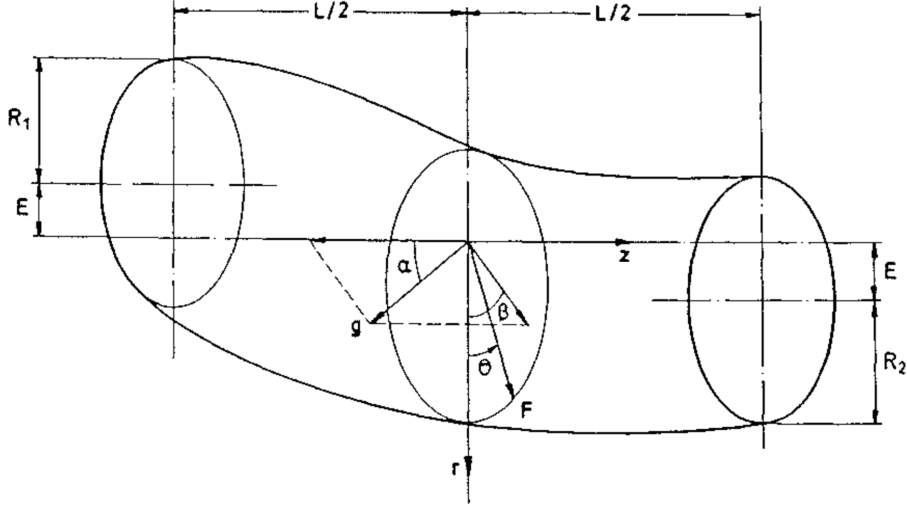


Figure 2.2: Geometry and coordinate system of a generic liquid bridge

The two circular end-disks can have different radii R_1 and R_2 with an eccentricity $2E$, and can be separated to form a gap of reduced distance L . The liquid bridge has a density ρ , a surface tension γ , and holds a volume of liquid V . Other important parameters are the gravity g , divided into axial g_z and lateral g_l component, the pressure jump p at the interface and the kinematic viscosity ν of the liquid.

Such fluid configuration can be uniquely defined by the following set of dimensionless parameters: the **slenderness** $\Lambda = L/2R_0$, where $R_0 = (R_1 + R_2)/2$ is the mean radius, which is used as characteristic length; the **dimensionless volume** $V/(\pi R_0^2 L)$ defined as the ratio of the physical volume of the liquid bridge to the volume of a cylinder of the same length and radius; the **dimensionless eccentricity** $e = E/R_0$; the **Bond number** $B = \rho g R_0^2 / \gamma$ which is a measure of the ratio between gravitational and surface forces; the **Weber number** $We = \rho R_0 u_0 / \gamma$ which is a measure of the relative importance of the fluid's inertia compared to its surface tension, where u_0 is the velocity at the inlet; the **Ohnesorge number** $Oh = \nu / (\sqrt{\rho \gamma R_0})$ which is the ratio between the viscous force and the inertia

and surface forces.

Because of the large number of parameters involved, a complete study of the equilibrium shape and stability limits of liquid bridges is a very hard task. In this work, we consider an axisymmetric configuration ($e = g_t = 0$) with equal solid disks ($R_1 = R_2 = R_0$) and no axial acceleration (g_z) as sketched in figure 2.3.

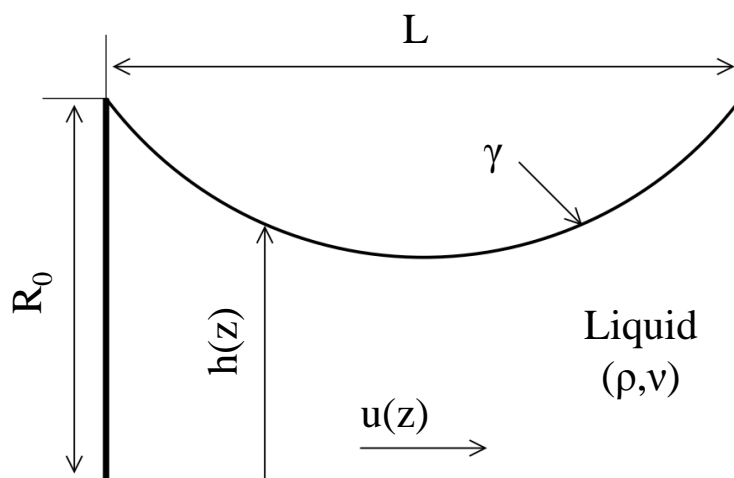


Figure 2.3: Sketch of liquid bridge model

2.2 The mathematical formulation

From the mathematical point of view, shapes of liquid bridges are described by the full Navier-Stokes equation with free surface boundary conditions; unfortunately this is very complicated, for both analytical and numerical studies since the zone about to pinch off requires very high resolution. Thus, a reduction of the physical problem to an easier model will give huge savings in computer time, this better approaching the singularity. There already exist some one-dimensional equations for axi-symmetric free surface flows ([3, 8, 13]). Our choice falls on the one-dimensional model developed by Eggers and Dupont [8] due to its simple but efficient structure.

The model starts from the Navier-Stokes equations in cylindrical coordinates for an axisymmetric column of fluid, i.e.

$$\frac{\partial u_r}{\partial t} + u_r \frac{\partial u_r}{\partial r} + u_z \frac{\partial u_r}{\partial z} = -\frac{1}{\rho} \frac{\partial p}{\partial r} + \nu \left(\frac{\partial^2 u_r}{\partial r^2} + \frac{\partial^2 u_r}{\partial z^2} + \frac{1}{r} \frac{\partial u_r}{\partial r} - \frac{u_r}{r^2} \right) \quad (2.1a)$$

$$\frac{\partial u_z}{\partial t} + u_r \frac{\partial u_z}{\partial r} + u_z \frac{\partial u_z}{\partial z} = -\frac{1}{\rho} \frac{\partial p}{\partial z} + \nu \left(\frac{\partial^2 u_z}{\partial r^2} + \frac{\partial^2 u_z}{\partial z^2} + \frac{1}{r} \frac{\partial u_z}{\partial r} \right) - g \quad (2.1b)$$

where u_z is the velocity along the axis, u_r the velocity along the radial direction, and the continuity equation

$$\frac{\partial u_r}{\partial r} + \frac{\partial u_z}{\partial z} + \frac{u_r}{r} = 0. \quad (2.2)$$

To equation (2.1) and (2.2) we have to add the balance of normal forces

$$\mathbf{n} \cdot \boldsymbol{\sigma} \cdot \mathbf{n} = -\gamma \left(\frac{1}{R_1} + \frac{1}{R_2} \right) \quad (2.3)$$

and tangential forces

$$\mathbf{n} \cdot \boldsymbol{\sigma} \cdot \mathbf{t} = 0 \quad (2.4)$$

where $\boldsymbol{\sigma}$ is the stress tensor, \mathbf{n} is the outward normal, R_1 and R_2 are the principal radii of curvature.

Finally, the surface has to move with the velocity field at the boundary

$$\frac{\partial h}{\partial t} + u_z \frac{\partial h}{\partial z} = v_r|_{r=h} \quad (2.5)$$

where $h(z, t)$ is the radial coordinate of the interface.

Using the Taylor series to expand with respect to r and solving the equation to lowest order in r , it is easy to obtain *the Eggers-Dupont one-dimensional model*:

$$\partial_t u = -uu_z - \frac{p_z}{\rho} + \frac{3\nu(h^2 u_z)}{h^2} \quad (2.6a)$$

$$p = \gamma \left[\frac{1}{h(1+h_z^2)^{1/2}} - \frac{h_{zz}}{(1+h_z^2)^{3/2}} \right] \quad (2.6b)$$

$$\partial_t h = -uh_z - \frac{1}{2}u_z h \quad (2.6c)$$

where the subscript "z" denotes the partial derivative with respect to z .

This set of equations (2.6) has to be solved for $z \in [0, L]$ imposing the following boundary conditions:

$$h(0) = h(L) = R_0 \quad (2.7a)$$

$$u(0) = u(L) = u_0 \quad (2.7b)$$

For this simplified system, the mass conservation law has to be imposed:

$$V = \pi \int_0^L h^2 dz \quad (2.8)$$

The set of equation (2.6), (2.7) and (2.8) will concern us for the rest of this work.

3 Bifurcation theory

A *bifurcation* of a dynamical system is a qualitative change in its dynamics produced by varying parameters. A bifurcation occurs when a smooth change made to the parameter values (the *bifurcation parameters*) of a system causes a sudden "qualitative" or topological change in its behaviour. One goal of bifurcation theory is to produce parameter space maps or *bifurcation diagrams* that shows the possible long-term values (equilibria/fixed points or periodic orbits) of a system as a function of a bifurcation parameter in the system. Two examples of bifurcation diagrams with different axes are presented in figure 3.1 and 3.2.

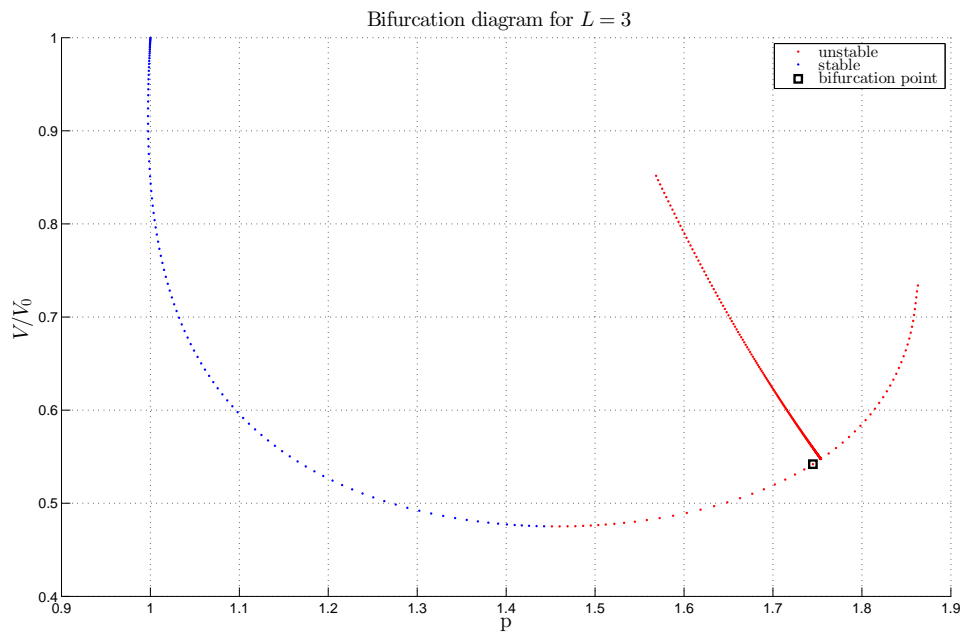


Figure 3.1: Volume-pressure bifurcation diagram for vanishing Weber number

3.1 Stationary solution

A first step in the bifurcation analysis consists in determining the stationary solution branches of equations (2.6). Let $x = (u, h)$ be the state variable, in

vector notation equations (2.6) can be written as $\dot{x} = f(x)$. *Equilibrium* points, also called *stationary* solutions, $x_s = (u_s, h_s)$ are points where the system remains in the same state as time elapses, in every observable way. Then, they are defined by $\dot{x} = 0$ and satisfy the equation

$$f(x_s) = 0$$

In our case, stationary states of (2.6) are solutions of the algebraic system:

$$-uu_z - \frac{p_z}{\rho} + \frac{3\nu(h^2u_z)}{h^2} = 0 \quad (3.1a)$$

$$-uh_z - \frac{1}{2}u_z h = 0 \quad (3.1b)$$

where

$$p = \gamma \left[\frac{1}{h(1+h_z^2)} - \frac{h_{zz}}{(1+h_z^2)} \right]$$

with its boundary conditions and mass conservation property:

$$h(0) = h(L) = R_0 \quad (3.2)$$

$$u(0) = u(L) = u_0 \quad (3.3)$$

$$V = \pi \int_0^L h^2 dz \quad (3.4)$$

Every parameter in (3.1) can be use as *bifurcation parameter* in order to build a *bifurcation diagram*. The curves in diagrams of figure 3.1 and 3.2 represent the *branches* of solutions to (3.1), i.e., the equilibria point of system (2.6).

3.2 Bifurcation diagram

The purpose of the diagram is to display qualitative information about equilibria, across all equations $\dot{x} = f(x)$, obtained by varying physical parameters appearing in f . An example of bifurcation diagram of system (3.1) using the Weber number as bifurcation parameter is presented in figure 3.2. However, it has long been

realized that once a bifurcation diagram has been determined, either numerically or analytically, certain conclusion concerning stability proprieties can be made with little or no additional analysis.

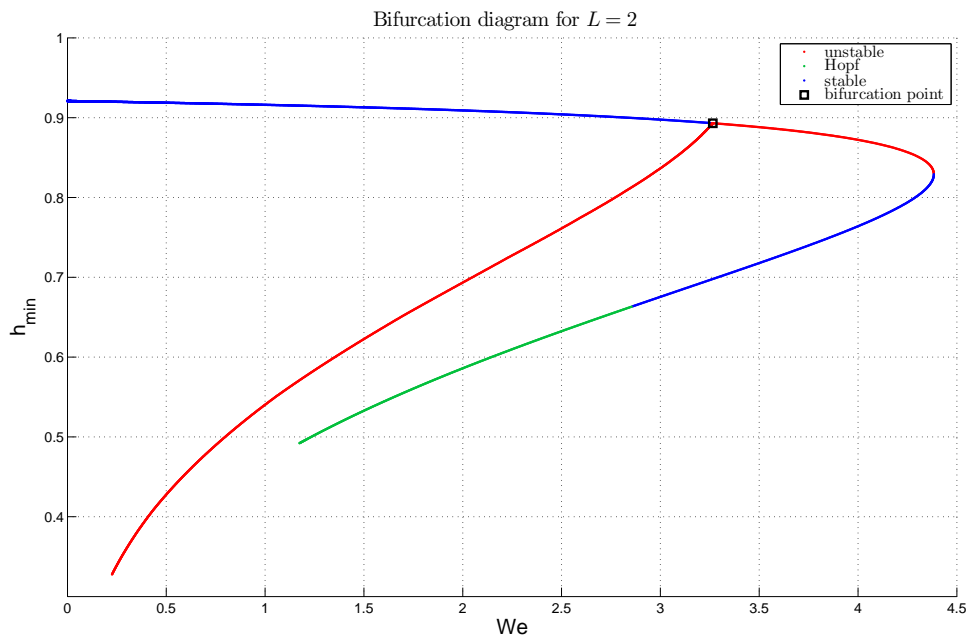


Figure 3.2: Minimum radius-Weber number bifurcation diagram

Maddocks in [16] demonstrates that the stability can be determined by examining equilibria in the bifurcation diagram. It is well known from bifurcation theory that if a stable branch undergoes a turning point, then there is a change in stability at the turning point. Maddocks further says that, in preferred coordinates, each turning point involves a change in sign of an eigenvalue and, moreover, it gives criteria to specify that change (e.g. plus to minus).

The theorem by Maddocks [16] considers minimization problems of the form

$$F(u) = G(u) - \lambda H(u)$$

where F is a functional and G is the object to minimize subject to H prescribe

(the constrained problem) or subject to λ prescribed (the unconstrained problem) and demonstrate (see figure 3.3):

Theorem (Maddocks) *Consider solution curves in the $H - \lambda$ preferred diagram with a simple fold and without branch points. For the unconstrained problem, as the fold is traversed (decreasing H), the number of negative eigenvalues of the Jacobi equation changes from k to $k + 1$ if the fold opens to the right and from k to $k - 1$ if the fold opens to the left. For the constrained problem, as the fold is traversed (increasing A), the number of negative eigenvalues changes from j to $j + 1$ if the fold opens upward and from j to $j - 1$ if the fold opens downward.*

In our case, the exact surface of static equilibrium is also an equilibrium surface of the model (2.6) which minimizes the potential energy of the system.

In this work, we have developed a first case where the system is subject to a prescribed volume $V = \text{constant}$ that leads to take the pressure as bifurcation parameter. In the second case the system is subject to a prescribed Weber number using the shape of the interface as parameter.

3.3 Singular point

A local bifurcation occurs when a parameter change causes the stability of an equilibrium (or fixed point) to change and it is called *bifurcation point*.

There are different types of bifurcations. We start with a classification of the different local bifurcations, that is, the bifurcations that involve equilibria. These bifurcations can be classified in terms of the eigenvalues of the Jacobian matrix associated with the (parameter-dependent) equilibrium.

Hence, we can think of the bifurcation as a movement of eigenvalue(s) through the imaginary axis as a parameter is varied. For vector fields, there are two generic cases: either one eigenvalue moves through the origin, or a pair of complex conjugated eigenvalues moves through the imaginary axis.

Examples of local bifurcation that appear in figure 3.2 are:

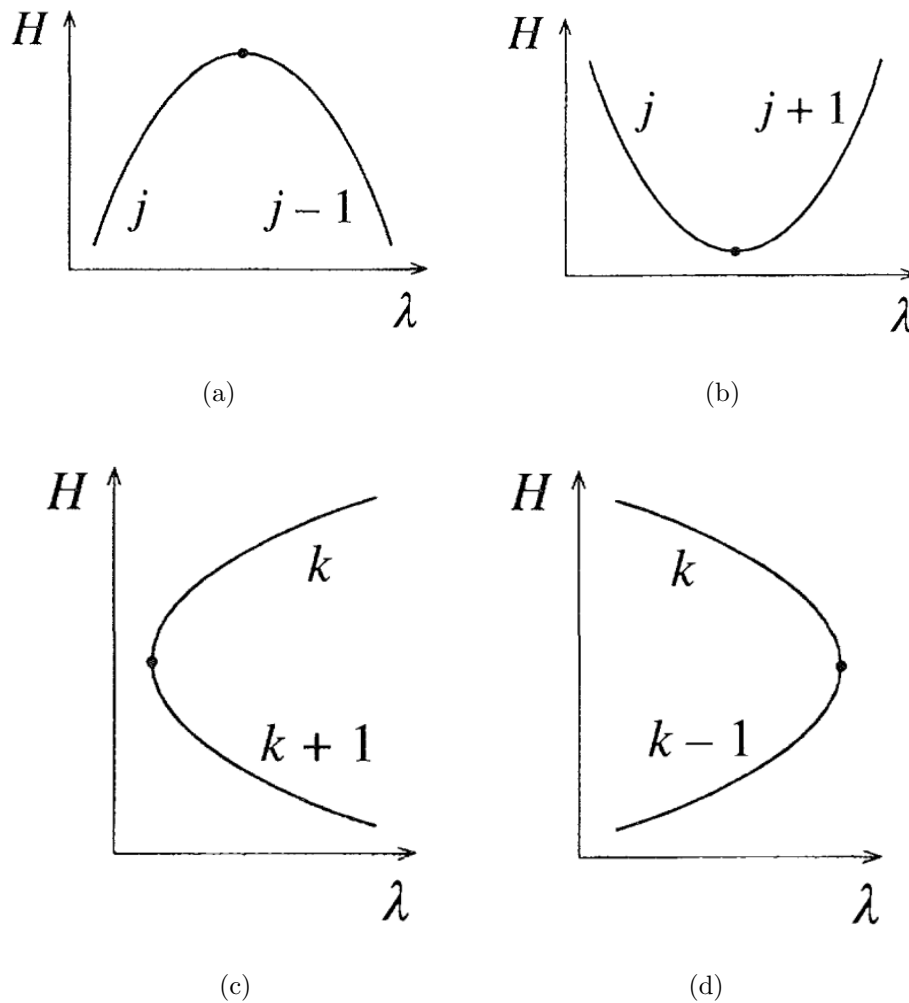


Figure 3.3: Change in number of negative eigenvalues at a turning point, for the constrained (figure *a* and *b*) and unconstrained (figure *c* and *d*) problems, respectively

Saddle-node (fold) bifurcation The saddle-node bifurcation is characterised by the fact that on one side of the bifurcation two equilibria exist, while on the other side of the bifurcation these two equilibria disappear. This bifurcation is localized where the branch curve turns back and it is associated to one eigenvalue "moving through" the origin. The bifurcation

point can be thought of as the point where the two equilibria collide. The saddle-node bifurcation can take place in any system and is, in fact, a very typical bifurcation to happen when a parameter is varied. Maybe because this bifurcation is so typical, it has a lot of other names like *fold bifurcation*, *tangent bifurcation*, *limit point bifurcation* or *turning point bifurcation*. In figure 3.2 the turning point bifurcation is marked with **F**;

Hopf bifurcation In the mathematical theory of bifurcations, a *Hopf or Poincaré-Andronov-Hopf bifurcation*, named after Henri Poincaré, Eberhard Hopf, and Aleksandr Andronov, is a local bifurcation in which a fixed point of a dynamical system loses stability as a pair of complex conjugate eigenvalues of the linearised system around the fixed point cross the imaginary axis of the complex plane. (points **H**);

Branch point is where two different branches intersect (point **B**).

4 Linear stability analysis

Stability theory studies the stability of a dynamical systems under small perturbations of initial conditions. Stability means that the system goes back to its original state after it is submitted to a small external perturbation. Formally, a stationary solution x_s is *stable* if, starting from initial values $x(t)$ that are sufficiently close to the equilibrium, the system approaches the steady state as time goes to infinity

$$x(t) \xrightarrow{t \rightarrow \infty} x_s$$

Otherwise, the response tend to grow and the stationary solution is called *unstable*.

A classical example of stable state is a ball in a bowl, as shown in figure 4.1(a). If we move the ball from the original state to a disturbed state, after some oscillations it goes back to its original state. On the other hand, a ball on a hilltop (figure 4.1(b)) is an unstable state because every disturbance will produce an ever-increasing change from the original state.

Before we begin the analysis of our problem, it is worth to outline the basic general procedure involved in a linear stability analysis:

1. specify the governing non-linear equations and related boundary conditions;
2. find the steady state;
3. subject the steady state to a small perturbation of order δ ;
4. linearise the equations: substitute the perturbed form into the governing equations, expand in Taylor series with respect to the perturbation δ around the steady state and neglect second order term $O(\delta^2)$ and higher;
5. analyse the eigenvalue of the Jacobian matrix J to find stable and unstable steady states.

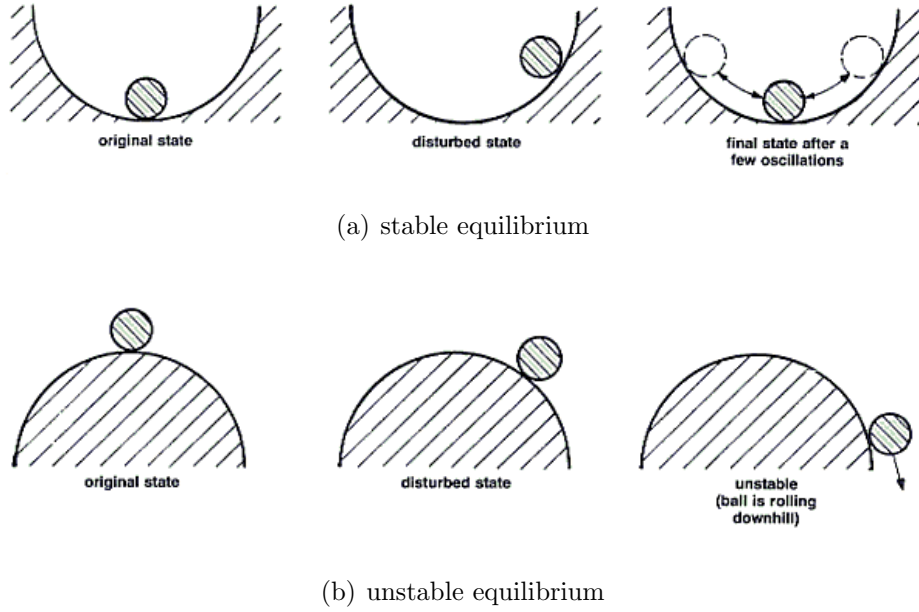


Figure 4.1: Classical example of stability

4.1 The linearisation

In our case, the governing equations are the set (2.6) presented in section 2.2.

Let $x = (u, h, p)$ be the state vector and $x_0 = (U, H, P)$ an equilibrium point. To linearise the governing equations, we add a small perturbation δx to the stationary point x_0 and substitute the perturbed state into the governing equations, the perturbed state is:

$$u \rightarrow U + \delta u \quad (4.1)$$

$$h \rightarrow H + \delta h \quad (4.2)$$

$$p \rightarrow P + \delta p, \quad (4.3)$$

and the governing equations (2.6) become

$$\begin{aligned} \partial_t(U + \delta u) = & - (U + \delta u)(U_z + \delta u_z) - \frac{(P + \delta p)_z}{\rho} + \\ & + \frac{3\nu [(H + \delta h)^2(U + \delta u)_z]}{(H + \delta h)^2} \end{aligned} \quad (4.4a)$$

$$(P + \delta p) = \gamma \left\{ \frac{1}{(H + \delta h) [1 + (H + \delta h)_z^2]^{1/2}} - \frac{(H + \delta h)_{zz}}{[1 + (H + \delta h)_z^2]^{3/2}} \right\} \quad (4.4b)$$

$$\partial_t(H + \delta h) = - (U + \delta u)(H + \delta h)_z - \frac{1}{2}(U + \delta u)_z(H + \delta h). \quad (4.4c)$$

Recalling the first order Taylor series

$$(1 + x)^\alpha = 1 + \alpha x$$

with $\alpha \in \mathbb{R}$, the expansions of some term in equation (4.4) are:

$$\frac{1}{(H + \delta h)^2} = \frac{1}{H^2 \left(1 + \frac{\delta h}{H}\right)^2} = \frac{1}{H^2} \left(1 - 2\frac{\delta h}{H}\right) \quad (4.5)$$

$$\begin{aligned} \frac{1}{[1 + (H_z + \delta h_z)^2]^{1/2}} &= \frac{1}{(1 + H_z^2 + 2H_z\delta h_z)^{1/2}} = \\ &= \frac{1}{(1 + H_z^2)^{1/2} \left(1 + \frac{2H_z\delta h_z}{1 + H_z^2}\right)^{1/2}} = \frac{1}{(1 + H_z^2)^{1/2}} \left(1 - \frac{H_z\delta h_z}{1 + H_z^2}\right) \end{aligned} \quad (4.6)$$

In the same way as before we can achieve:

$$\frac{1}{(H + \delta h)} = \frac{1}{H} \left(1 - \frac{\delta h}{H}\right) \quad (4.7)$$

$$\frac{1}{[1 + (H_z + \delta h_z)^2]^{3/2}} = \frac{1}{(1 + H_z^2)^{3/2}} \left(1 - 3 \frac{H_z \delta h_z}{1 + H_z^2} \right) \quad (4.8)$$

Substituting expansion (4.5)-(4.8) in equations (4.4), and neglecting second order terms and higher, we finally arrived at *the linearised equation*:

$$\begin{aligned} \frac{\partial \delta u}{\partial t} = & -U \delta u_z - U_z \delta u - \frac{\delta p_z}{\rho} - \frac{6\nu H_z U_z}{H^2} \delta h + \\ & + \frac{6\nu U_z}{H} \delta h_z - \frac{6\nu H_z}{H} \delta u_z + 3\nu \delta u_{zz} \end{aligned} \quad (4.9a)$$

$$\frac{\partial \delta h}{\partial t} = -U \delta h_z - U_z \delta h - \frac{1}{2} H \delta u_z h - \frac{1}{2} U_z \delta h \quad (4.9b)$$

with

$$\delta p = \gamma \left[-\frac{1}{H^2 a^{1/2}} \delta h - \left(\frac{H_z}{H a^{3/2}} - \frac{3H_z H_{zz}}{a^{5/2}} \right) \delta h_z - \frac{1}{a^{3/2}} \delta h_{zz} \right]$$

calling $a = 1 + H_z^2$.

4.2 The stability analysis

The study of the stability of a non-linear dynamic system start with the the study of the linearised system

$$\dot{x} = Ax \quad (4.10)$$

where A is a linear operator. In our case, A is represented by the linearisation (4.9)

$$A = \begin{bmatrix} -U_z + \left(\frac{6\nu H_z}{H} - U \right) \frac{\partial}{\partial z} & \frac{1}{\rho} \frac{\partial L}{\partial z} - \frac{6\nu H_z U_z}{H} + \left(\frac{6\nu U_z}{h} \right) \frac{\partial}{\partial z} \\ -H_z - \frac{1}{2} H \frac{\partial}{\partial z} & -\frac{1}{2} U_z - U \frac{\partial}{\partial z} \end{bmatrix} \quad (4.11)$$

with

$$L = \gamma \left[-\frac{1}{H^2 a^{1/2}} - \left(\frac{H_z}{H a^{3/2}} - \frac{3H_z H_{zz}}{a^{5/2}} \right) \frac{\partial}{\partial z} - \frac{1}{a^{3/2}} \frac{\partial^2}{\partial z^2} \right]$$

is the differential operator from the pressure equation.

The main purpose in studying the stability of a dynamical system is to know whether a perturbation of solution grows, stays constant or shrinks as $t \rightarrow \infty$. This can usually be answered just by examining the eigenvalues of the linear

operator A :

- if all eigenvalues s have strictly negative real part, then all solutions of (4.10) approach zero exponentially and the equilibrium point x_0 is considered *stable*;
- if at least one eigenvalue has a positive real part, the majority of solutions of the linearised system grows exponentially and x_0 is *unstable*;
- If some pairs of complex-conjugate eigenvalues have zero real parts with distinct imaginary parts, then the corresponding solutions oscillate and neither decay nor grow as $t \rightarrow \infty$.

4.3 Stability diagram

A typical linear stability curve for the limit case without acceleration ($Bo = 0$) is shown in figure 4.2 (dashed line). For axisymmetric liquid bridges with $e = Bo = We = 0$ and equal disks, early stability studies were published more than 20 year age by Gillette and Dayson [10]. Later studies on axisymmetric perturbations by Martinez [17, 23] and on arbitrary perturbations by Slobozhanin [25, 26] led to the construction of the stability region.

According to these works, the boundary of the stability region in the $\Lambda - V$ plane is unclosed and consist of three parts. On the upper boundary the bridge looses its stability with respect to non-axisymmetric perturbations. The maximum volume limit is determined by a non-axisymmetric deformation of the liquid bridge interface and a possible spreading of the liquid over the lateral surfaces of the end-disks. On the lower boundary, the minimum volume stability limit is driven by an axisymmetric perturbation. For large slenderness, $\Lambda > 2.13$, on the right part of boundary, the stability limit is determined by the appearance of a pitch-fork bifurcation to unstable equilibrium with non-symmetric shape with respect to the middle plane parallel to the disks. This means that when the stability limit is reached, the breakage of the liquid bridge causes two drops of different volume. On the left part of the boundary a detachment is characterized

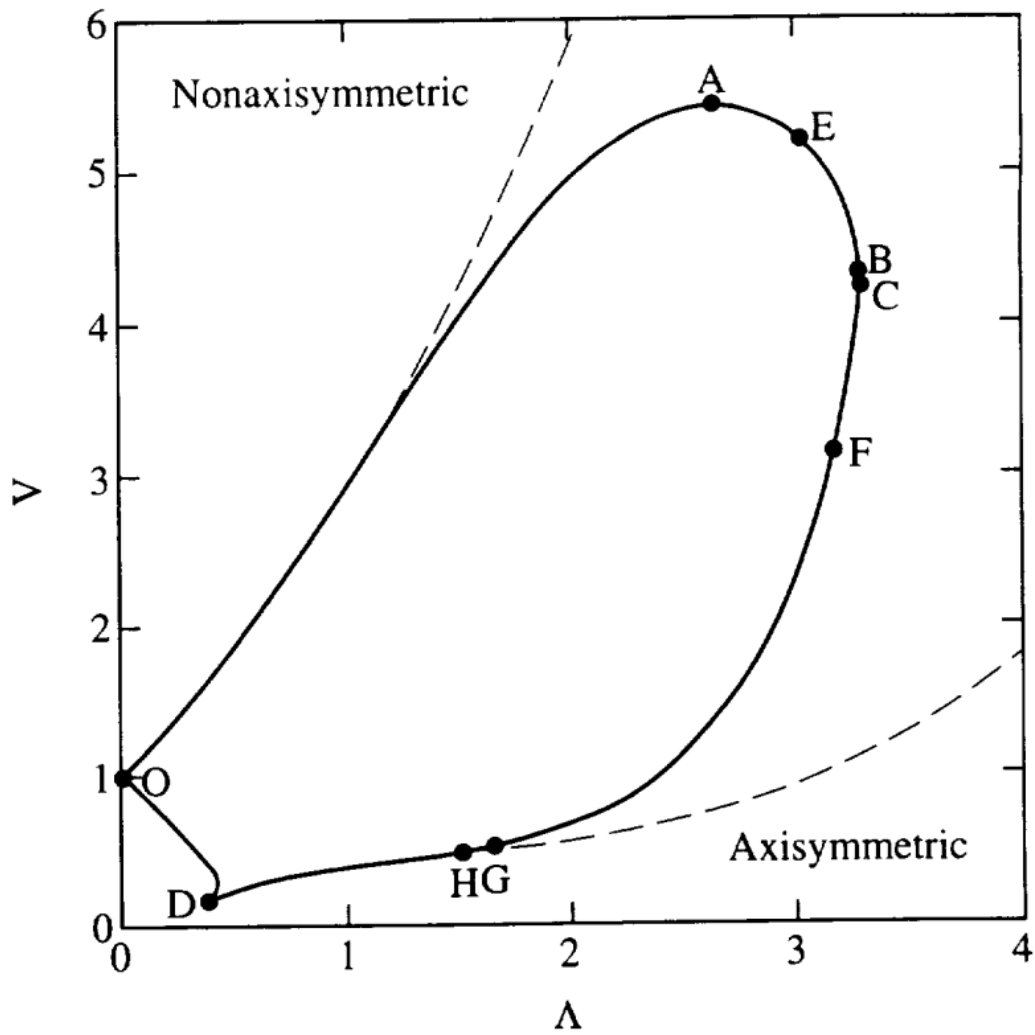


Figure 4.2: Typical stability diagram of liquid bridges between equal disks with small constant axial acceleration ($Bo = 0.1$ solid line) and no acceleration ($Bo = 0$ dashed line) [Slobozhanin and Perales [27]]

by small slenderness ($\Lambda < 2.31$); the stability limit is due to a turning point in the bifurcation diagram and the associated unstable equilibrium shapes are still symmetric with respect to the middle plane parallel to the disks. The corresponding drops appearing after the breaking will be of equal size. Finally, if the slenderness is small enough, there is another minimum limit volume due to a possible detachment of liquid bridge interface from the edges of disks (curve OD).

The influence of axial gravity on the character of deformation of the first and second parts of the boundary corresponding to $Bo = 0$ was determined by Barmin et al. [2]. According to the results mentioned above, for each non-zero value of the Bond number the stability diagram of capillary liquid bridges can be represented by a single closed piecewise curve on the $\Lambda - V$ plane.

Liquid bridge configurations represented by points inside the region bounded by this curve are stable whereas those lying outside are unstable. A typical stability limit curve for small Bond numbers ($Bo = 0.1$) is shown in figure 4.2 with a solid line. In such a stability limit it is possible to distinguish three different parts. For volumes $V < 1$ and small slenderness, the instability is governed by the detachment of the interface (the wetting line) from the edges of the top disk (curve OD in figure 4.2 corresponds to zero wetting angle). Another part of the stability limit curve, corresponding to a minimum in the volume, is characterized by the axisymmetric breakage of the liquid bridge (curve DC where point C is always below the point of maximum slenderness B), such a part of the stability curve being known in the literature as the minimum volume stability limit. Finally, the last part of the curve (curve OABC) is characterized by the loss of axisymmetry of the equilibrium shapes, i.e., a non-axisymmetric deformation appears.

5 Numerical procedure

In this section we will present the numerical methods to develop a MATLAB code. Particularly, we illustrate the numerical techniques used in the analysis of bifurcation and the method used to perform the continuation of solutions.

The numerical approximation were computed using an algorithm that builds the differentiation matrix using the spectral collocation method based on Chebyshev polynomial [28].

5.1 The NewtonRaphson method

As presented in section 3.1, in bifurcation analysis the first thing to do is finding the stationary solution branches (or solution paths). Stationary solution x_s are defined as solutions of the (non-linear) vector equation $f(x) = 0$. The classical way to solve this problem is the *NewtonRaphson method* that let you find successively better approximations to the zeroes of a real-values function.

Through a linearisation of f using Taylor series expansion, one obtains

$$0 = f(x_s) \approx f(x_0) + f'(x_0) \cdot (x_s - x_0)$$

where x_0 is an approximation of x_s and $f'(x_0)$ is the Jacobian matrix evaluated at x_0 . The above relation set a way to a better approximation x_1 by solving

$$x_1 = x_0 - \frac{f(x_0)}{f'(x_0)} \quad (5.1)$$

Applying equation (5.1) repeatedly produces a series of better approximation

$$x_1, x_2, x_3, \dots$$

Under certain assumptions (the most important of which is non-singularity of the Jacobian at the solution), one can guarantee *quadratic* convergence in a neighbourhood of the solution. This means that both $f(x_n)$ and $x_s - x_n$ go

quickly to zero. In practice, however, the usual assumptions ensuring this rate of convergence are not always satisfied. Therefore we often encounter limitations on the rate of convergence.

The main limitation is due to the initial guess. For many difficult problems an arbitrary initial guess x_0 does not lead to convergence of the sequence produced by equation (5.1) because x_0 may be too far away from a solution.

There are lot of technique to improve the convergence efficiency of the NewtonRaphson method. Our choice falls on using a continuation method to predict the initial guess from previous solutions. This method will be presented better in next section.

5.2 Continuation of solution - Pseudo-arclength continuation

Numerical continuation is a technique to compute a consecutive sequence of points which approximate the desired branch. The idea behind this method is to generate the next point x_{i+1} making a prediction from a found point x_i on the curve. Then the predicted point is corrected to satisfying a chosen tolerance criterion $\|f(x_i)\| \leq \epsilon$ for some $\epsilon > 0$.

According to [5], one of the most popular continuation method is the *pseudo-arclength continuation*. It can be formulated as

$$f(x_1, \lambda_1) = 0, \quad (x_1 - x_0)^T \dot{x}_0 + (\lambda_1 - \lambda_0) \dot{\lambda}_0 - \Delta s = 0$$

that is a more useful approximation for computations of the arclength continuation.

Geometrically interpreted, this method finds a solution (x_1, λ_1) to $f(x, \lambda) = 0$ in a hyperplane that is at distance Δs from (x_0, λ_0) and that is perpendicular to the direction vector $(\dot{x}_0, \dot{\lambda}_0)$ as presented in figure 5.1.

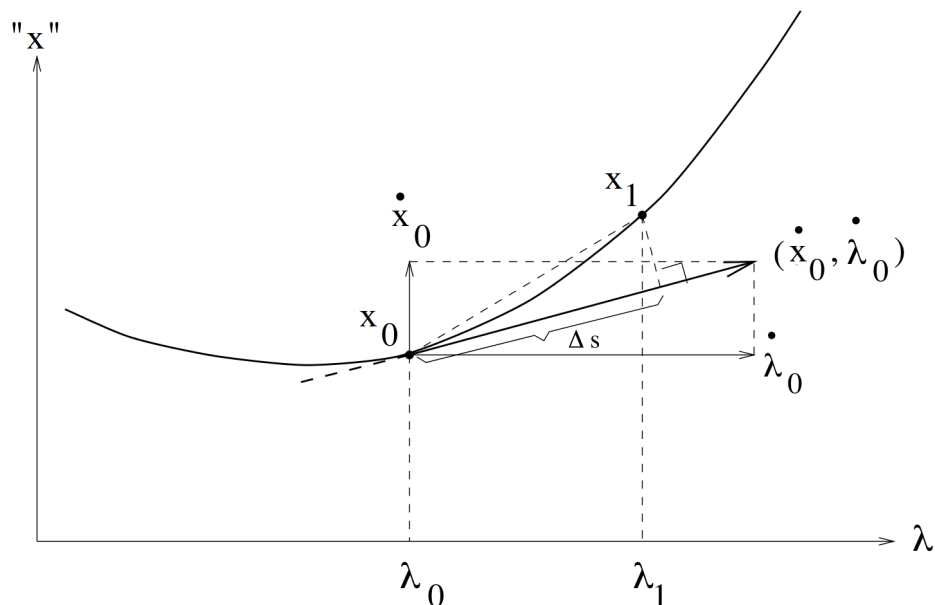


Figure 5.1: Graphical interpretation of pseudo-arclength continuation

5.3 Bifurcation point and branch switching

The location of bifurcation points is important to individuate secondary branch passing through our path. After the identification of a bifurcation point, the second direction has to be computed and the path switch to the second branch.

Let

$$F(x) = \begin{pmatrix} f(x) \\ (x - x_0)^T \dot{x}_0 - \Delta s \end{pmatrix}$$

and let x_0 be a bifurcation point, then

$$F_x = \begin{pmatrix} f_x \\ \dot{x}_0^T \end{pmatrix}$$

change sign at x_0 , as shown in [5]. The determinant of the Jacobian F_x is monitored along the solution branch. Points where determinant changes sign are marked as *bifurcation point* and the *branch switching method* is called to follow

the second branch.

Since x_0 is a simple singular point and $N(f_x(x_0)) = \text{Span}(\phi_1, \phi_2)$, the direction vector has the form of $\dot{x}_0 = \alpha_1\phi_1 + \beta_1\phi_2$. The direction of the bifurcation branch $x'_0 = \alpha_2\phi_1 + \beta_2\phi_2$ can be calculated evaluating α and β that correspond to the linearly independent solutions of the *Algebraic Bifurcation Equation* [Keller [12]]

$$c_{11}\alpha^2 + 2c_{12}\alpha\beta + c_{22}\beta^2 = 0$$

.

We can take ϕ_1 to be the direction of the "given" branch at the bifurcation point, i.e. $\phi_1 = \dot{x}_0$, and choose $\phi_2 \perp \phi_1$. Then ϕ_2 is a null vectors of $F_x(x_0)$.

Then, the first solution on the new bifurcation branch can be computed with the pseudo-archlength continuation method:

$$\begin{aligned} f(x) &= 0 \\ (x_1 - x_0)^T x'_0 - \Delta s &= 0 \end{aligned}$$

However, a less expensive in computer time and more efficient way to switch branch is to use the vector ϕ_2 rather than the real direction x'_0 (*orthogonal direction method*). The branch switching procedure then simply consists of computing the null vector ϕ_2 , followed by the pseudo-archlength continuation method:

$$\begin{aligned} f(x) &= 0 \\ (x_1 - x_0)^T \phi_2 - \Delta s &= 0 \end{aligned}$$

5.4 Step-size control

Step-size control is an important issue in these algorithms. Too small step-sizes lead to unnecessary work been done, while too big step-sizes can lead to losing details of the curve or finding any solution. An easy and reliable method is convergence-dependent control.

Consider the computation of a next point using step size δ_i . If the computation

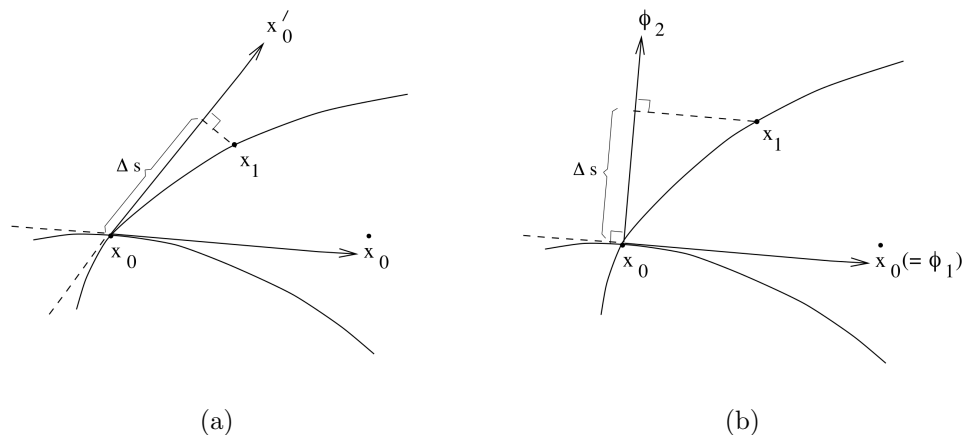


Figure 5.2: Comparison between the correct (a) and the orthogonal (b) direction

converged, let n denote the Newton iterations needed. Then the new step-size δ_{i+1} will be selected as follow

$$\delta_{i+1} = \begin{cases} \delta_i \cdot \delta_{dec} & \text{if not converged} \\ \delta_i \cdot \delta_{inc} & \text{if converged and } n < n_{min} \\ \delta_i & \text{otherwise} \end{cases}$$

5.5 Numerical differentiation

The evaluation of the Jacobian in equation (5.1) mostly is expensive. Because analytic expressions for the partial derivatives of f are often unavailable, implementations of the Newton method make use of *numerical differentiation*.

The simplest method is to use finite difference approximations. A simple two-point estimation is to compute the slope of a nearby secant line through the points $(x, f(x))$ and $(x + \epsilon, f(x + \epsilon))$. Choosing a small number ϵ that represents a small change in x , the slope of this line is

$$\frac{f(x + \epsilon) - f(x)}{\epsilon}$$

This expression is *Newton's difference quotient*. The slope of this secant line

differs from the slope of the tangent line by an amount that is approximately proportional to ϵ . As ϵ approaches zero, the slope of the secant line approaches the slope of the tangent line. Therefore, the true derivative of f at x is the limit of the value of the difference quotient as the secant lines get closer and closer to being a tangent line:

$$\frac{f(x + \epsilon) - f(x)}{\epsilon} \xrightarrow{\epsilon \rightarrow 0} f'(x)$$

The following algorithm can be used to calculate an approximation of $f'(x)$, let z^k be the k -th column of the Jacobian f' , U and V two auxiliary n -vectors:

Algorithm 1 Numerical differentiation

Evaluate $U = f(x)$
 Choose a small $\epsilon > 0$
for $k = 1$ **to** n **do**
 $x_k = x_k + \epsilon$
 Evaluate the vector $V = f(x)$
 $z^k = \frac{V - U}{\epsilon}$
end for

5.6 Code validation

A very important task in developing a code is the *validation*. The computational method is tested first by simulating the classical stability of a cylinder. In Particular, we compare our stability analysis with the analytical dispersion relation from Eggers and Dupont work [8].

They start with a cylinder of radius r_0 that receives a sinusoidal perturbation of wavelength $\lambda = 2\pi/k$; then

$$\begin{aligned} r(z, t) &= r_0 [1 + \epsilon(t) \cos(kz)] \\ v(z, t) &= \epsilon(t) v_0 \sin(kz) \end{aligned}$$

Assuming $\epsilon(t) = \epsilon_0 e^{\omega t}$, solving to lowest order in ϵ equation (2.6a) and (2.6c) give

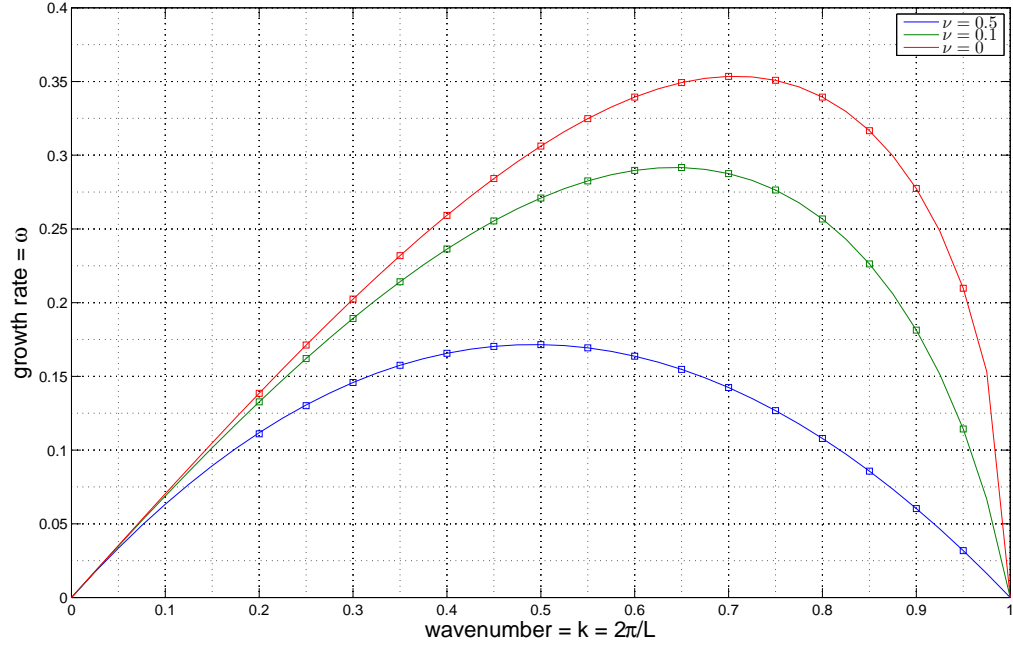


Figure 5.3: Comparison between code (square) and theory (line) for different value of viscosity

respectively

$$\omega v_0 = - \left(\frac{\gamma}{\rho} \right) \left(\frac{k}{r_0} - r_0 k^3 \right) - 3\nu v_0 k^2$$

$$\omega = -\frac{1}{2} v_0 k$$

that gives us the relation

$$\omega^2 = \omega_0^2 \frac{1}{2} [(r_0 k)^2 - (r_0 k)^4] - 3\nu \omega k^2 \quad (5.2)$$

$$\text{with } \omega_0^2 = \frac{\gamma}{r_0^3 \rho}$$

Solution of (5.2) gives the *dispersion relation*:

$$\omega = \omega_0 \left\{ \left[(kr_0)^2 \frac{1}{2} (1 - (kr_0)^2) + \frac{9 l_v}{4 r_0} (kr_0)^4 \right]^{\frac{1}{2}} - \frac{3}{2} \left(\frac{l_v}{r_0} \right)^{\frac{1}{2}} (kr_0)^2 \right\} \quad (5.3)$$

where $l_v = \nu^2 \rho / \gamma$ a viscous length-scale.

Our comparison with the dispersion relation (5.3) for three viscosity values is shown in figure 5.3. Our results fits perfectly the theory from [8]. As expected, there is an instability for wavelength longer than the perimeter, i.e. for wave-number less than $1/R_0$.

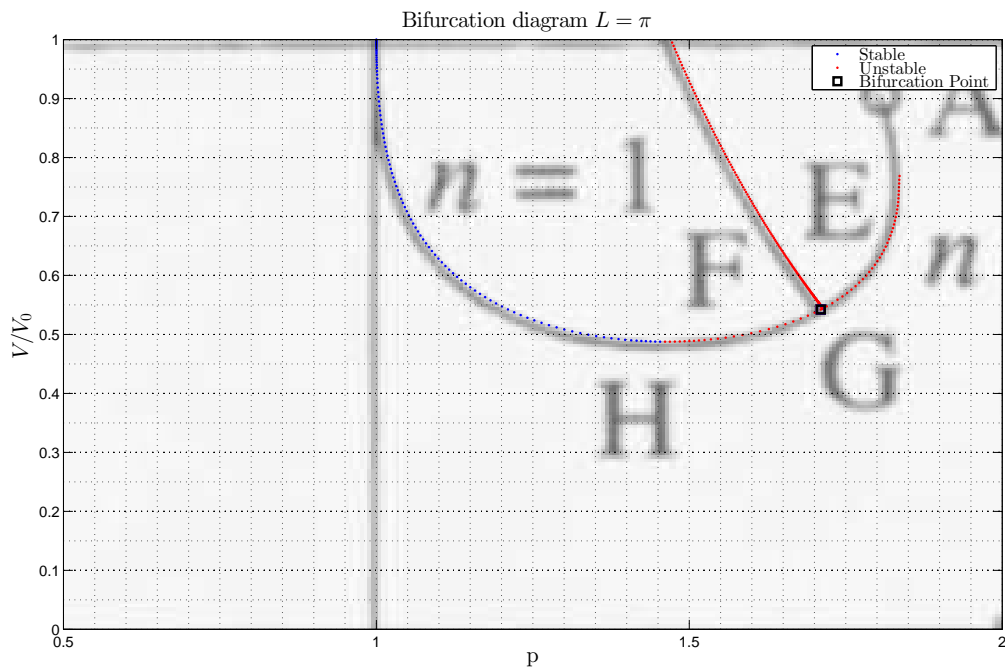


Figure 5.4: Comparison between our code and Lowry and Steen results [15]

The second step was comparing our continuations code with the bifurcation diagram done by Lowry and Steen in [15]. Figure 5.4 is an example of our comparison. As we can see, our results match very well the bifurcation curve

drawn by Lowry and Steen. Our code also predict very well the bifurcation point and the change in stability at the fold.

5.7 Code for integration in time

In this work has also been developed a time integration algorithm of the system (2.6). Due to the non-linear behaviour of the system, a combination of *finite difference method* and *Newton-Raphson method* has been used to follow the time evolution of the system.

Let now q be the state vector and f the non-linear function, system (2.6) can be rewrite as

$$\frac{\partial q}{\partial t} = f(q)$$

Using finite difference implicit method, previous equation become

$$\frac{q^{i+1} - q^i}{dt} = f(q^{i+1})$$

and finally

$$q^{i+1} + dt \cdot f(q^{i+1}) - q^i = 0 \quad (5.4)$$

Since f is not a linear function of q^{i+1} , equation (5.4) can not be rewrite with linear operator and solving in q^{i+1} . A way to do it is changing variable $q^{i+1} = q_0^{i+1} + \delta$ where q_0^{i+1} is a predicted next step solution and δ is a small variation. Then, we can rewrite the system as

$$q_0^{i+1} + \delta - dt \cdot f(q_0^{i+1} + \delta) - q^i = 0$$

Since δ is a small variation around q_0^{i+1} , we can use a linear approximation and $f(q_0^{i+1} + \delta)$ become $f(q_0^{i+1}) + J\delta$ where J is Jacobian matrix.

Then, the new equation can be written as

$$q_0^{i+1} + \delta - dt (f(q_0^{i+1}) + J\delta) - q^i = 0$$

$$\underbrace{q_0^{i+1} - dt \cdot f(q_0^{i+1}) - q^i}_A + \underbrace{(I - dt \cdot J)}_B \delta = 0 \quad (5.5)$$

Now, A and B are known as function of previous step solution and predicted next step solution. We have to add to equation 5.5 the boundary condition:

$$u(x = 0) = U(t) \quad (5.6a)$$

$$u(x = L) = U(t) \quad (5.6b)$$

$$h(x = 0) = R_0 \quad (5.6c)$$

$$h(x = L) = R_0 \quad (5.6d)$$

where R_0 is the end-disk radius of liquid bridge and $U(t)$ is function depending on time.

Value of δ can easily evaluate solving $\delta = A^{-1}(-B)$ and then the next-step state vector $q^{i+1} = q_0^{i+1} + \delta$. This have to be iterate till $F(q^{i+1}) = 0$ is satisfied. Then, q^{i+1} is the real next-step solution

The following algorithm is an example of time integration using this method

Algorithm 2 Time integration

Final time T

Time step Δt

Initial guess q_0

Tolerance tol

for $i = 0 : \Delta t : T$ **do**

Prediction next step solution q^{i+1}

while $A > tol$ **do**

Evaluate $A = q^{i+1} + \Delta t \cdot f(q^{i+1}) - q^i$

Evaluate $B = I - \Delta t \cdot J$

Adding boundary condition to A and B

$\delta = B^{-1}(-A)$

Correction of next step solution $q^{i+1} = q^{i+1} + \delta$

end while

end for

6 Simulation results

The aim of this thesis comes from recent studies by Hoepffner and Paré [11] who have studied the escape from pinch-off of a liquid filament. Our idea was to model the connection between the body of liquid and the drop as a liquid bridge and to study its stability for better understanding the phenomenon of "escaping". Then, our purpose was to build a MATLAB based code of the simplified one-dimensional model of liquid bridge presented in section 2.2 in order to analyse the stability and the influence of Ohnesorge and Weber numbers on the equilibrium points. Furthermore, a time-integration algorithm has been developed to dynamically simulate the evolution of liquid bridge to compare to quasi-static solutions done on GERRIS Flow Solver [1].

In the first part of this section, we analyse the influence of Weber number on the stability limit of liquid bridges. Our attention will be focused on the lower limit of the stability diagram, especially on thin bridges ($V < V_{cyl}$) with small slenderness $1 < \lambda < 3$. Finally, the quality of one-dimensional approximation in predicting the breakup of liquid bridge will be analysed in comparison with an axisymmetric model based on GERRIS Flow Solver.

6.1 Influence of Weber number on stability limit

In absence of acceleration and rotating velocity, it is well known that there is a critical slenderness for long cylindrical liquid bridges so that for Λ values smaller than critical, liquid bridges are stable. This stability limit, usually denoted the "Plateau-Rayleigh limit", occurs at $\Lambda = \pi$. The influence of centrifugal forces when the liquid bridge rotates as a solid body depends on the value of the Weber number and it has been analysed both theoretically and experimentally.

According to the stability limit [19], the *maximum stable slenderness* is

$$\Lambda_{crit} = \begin{cases} \frac{\pi}{(2We+1)^{1/2}} & We < \frac{1}{3} \\ \frac{\pi}{2We} & We > \frac{1}{3} \end{cases} \quad (6.1)$$

In figure 6.1 numerical results are presented on the maximum stable cylinder length L_{crit} compared to equation (6.1).

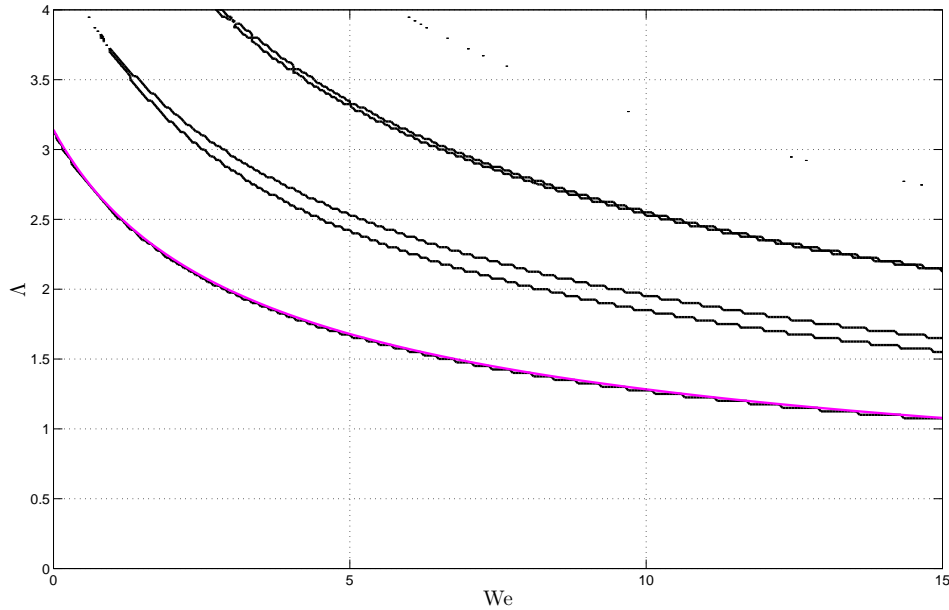


Figure 6.1: Influence of Weber number on the maximum stable cylinder length. Comparison between numerical result (black line) and equation (6.1)

As expected, the introduction of a Weber number based on the inlet flow velocity does not change the physics and our maximum stable slenderness is the same as that of a rotating liquid bridge. The approximation of the influence of Weber number based on inlet velocity on the well known stability limit for a cylindrical bridge $\Lambda = \pi$ appears to be valid for a larger range of values than shown in (6.1).

In general, the validity of equation (6.1) means that the system is unstable when the smallest phase speed on the bridge becomes less than the fluid velocity.

Another important aspect of our investigation is the influence of Weber number on the minimum volume stability limits. Diagrams in figure 6.2 show how Weber number shifts up the minimum volume limit on the bifurcation diagram.

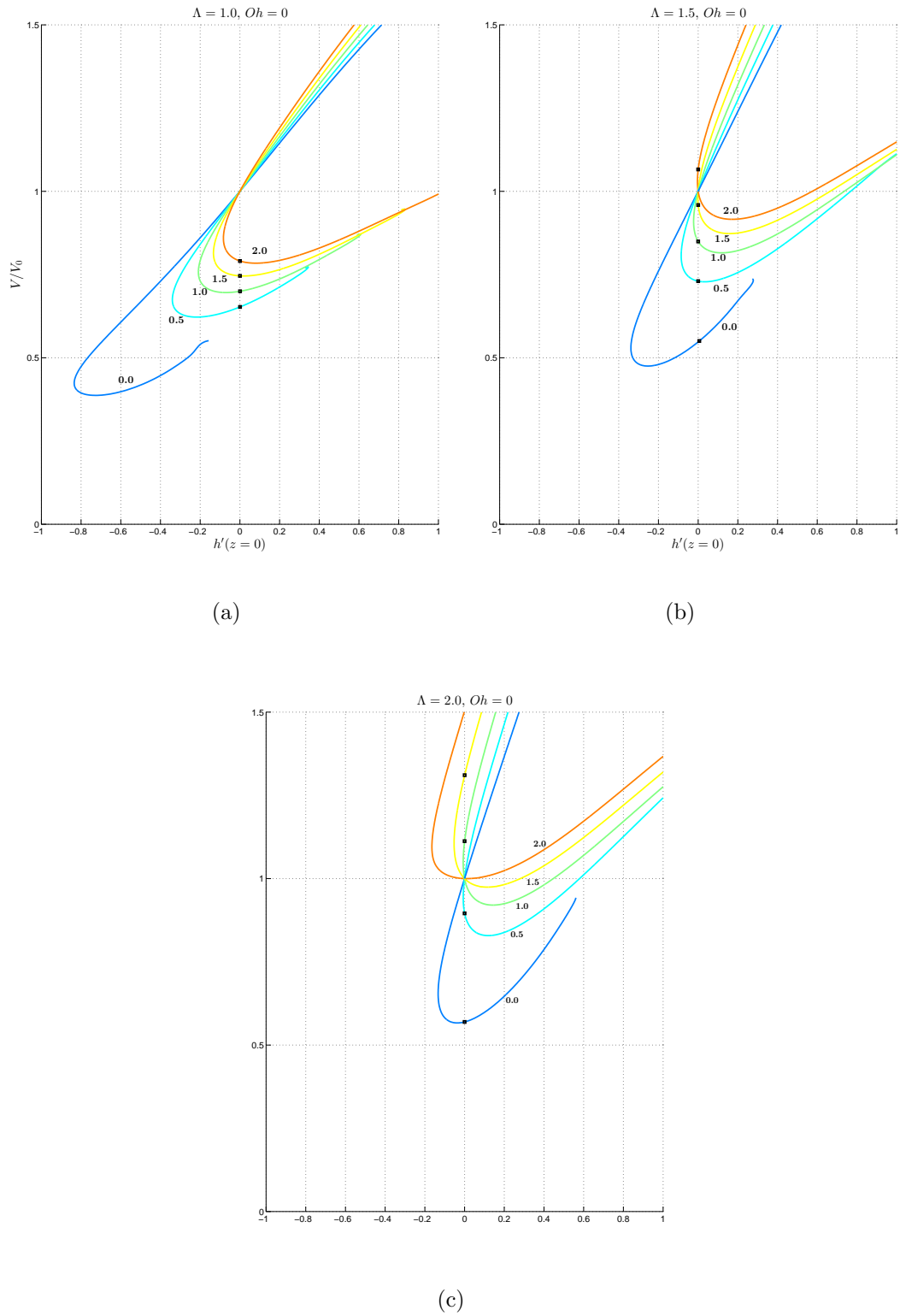


Figure 6.2: Influence of the Weber number on the bifurcation diagram for several slenderness. Numbers on the curves indicate the value of the Weber number

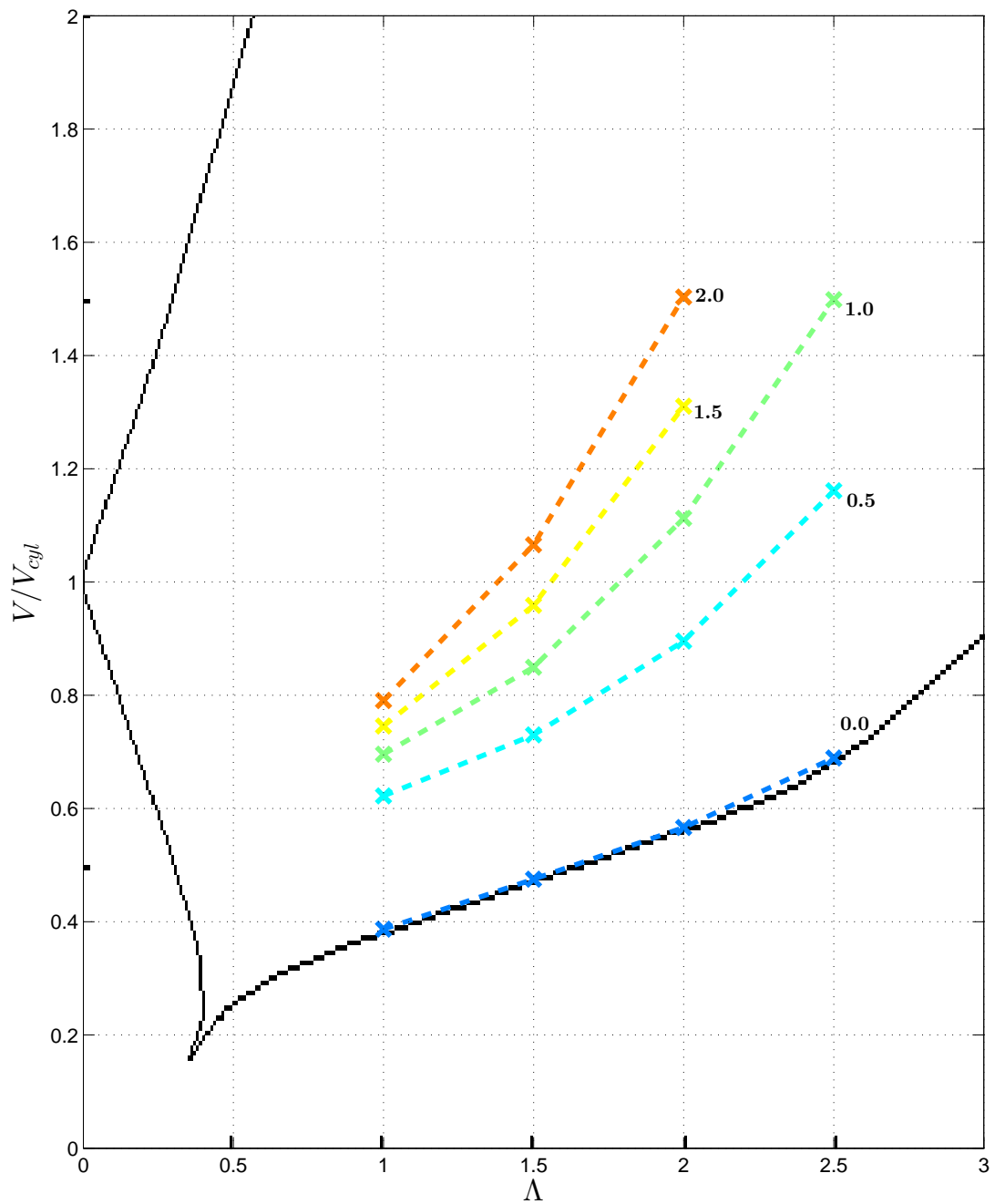


Figure 6.3: Minimum stable volume of liquid bridges. Numbers on the curves indicate the value of the Weber number

Results show that the presence of inlet flow velocity decreases the stability region in the $\Lambda - V$ plane, no matter the liquid bridge configuration is. In figure 6.3 the lower limit of stability diagram shift with variations of the Weber number is shown.

Another useful way to represent the bifurcation is to diagram a representative point of the equilibrium shape as a function of one bifurcation parameter.

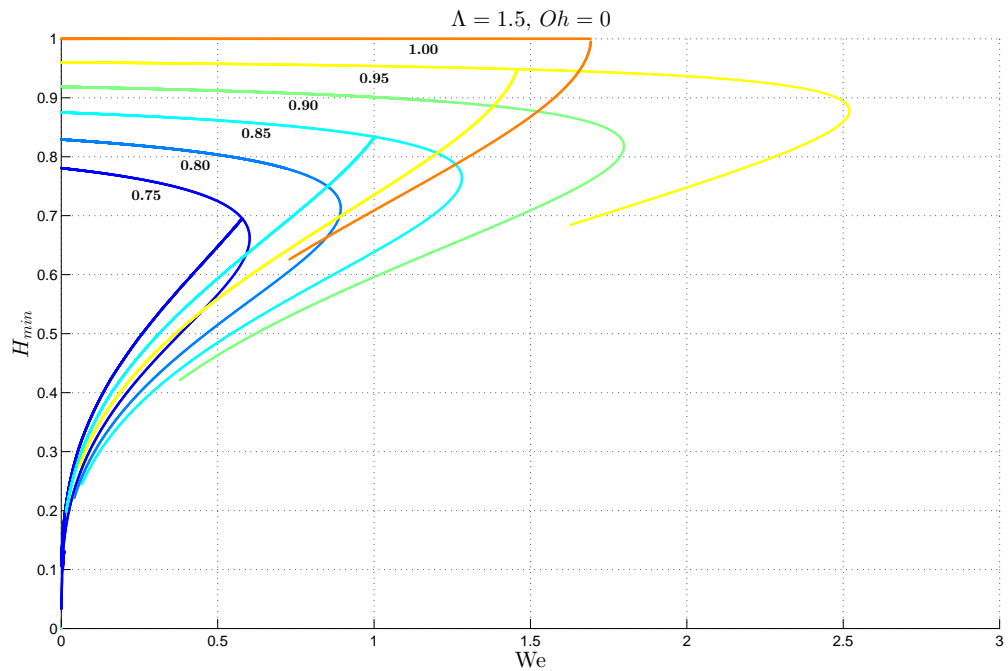
To characterise the shape in a single parameter one may use the extreme radius, i.e. the radius at the centre plane between discs, where the bulge or neck appears. However, it is better to use the radius at a quarter of the length, $R_{1/4}$, because this is also applicable to amphora-like deformations appearing with other loads and can give information on the symmetry of the shape. Another characteristic parameter that we use is the minimum radius of the liquid bridge because it gives information about the size of the neck. Figure 6.4 gives an example of the minimum radius as function of the Weber number, while figure 6.5(b) is an example of bifurcation using the radius at a quarter of the length as representative points.

In figure 6.5 the different equilibrium interfaces that can be observed in a liquid bridge by varying Weber number are presented. As can be easily seen in figure 6.5(a), the use of the minimum radius as characteristic parameter gives a better idea of the neck size. However, this parameter can not distinguish between two asymmetric shape which is possible using the radius at a quarter of the length 6.5(b).

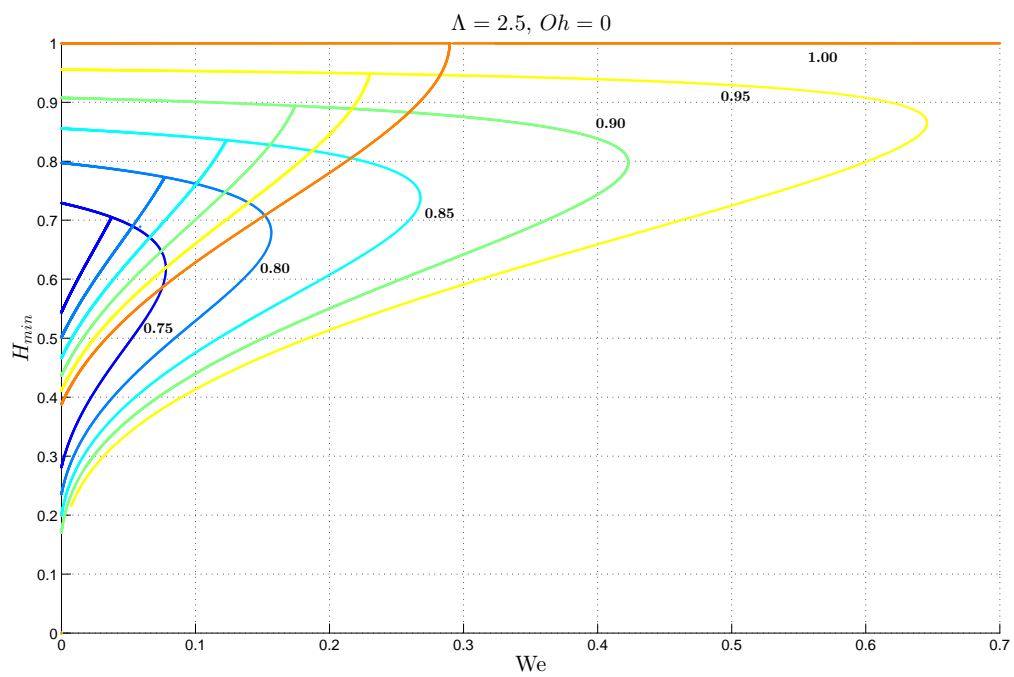
Two distinct branches have been identified, that can be better seen in figure 6.6.

6.2 Influence of Ohnesorge number (Oh)

Let us call *forward* the interface with minimum radius positioned downward along the flow and *backward* the interface with minimum upward (shape 3 and 4 of figure 6.5(c) respectively). The viscosity has an important role in changing the shape of the bifurcation diagram. In figure 6.6 how the viscosity modifies the bifurcation



(a)



(b)

Figure 6.4: Examples of bifurcation diagrams. Numbers on the curve indicate the value of volume

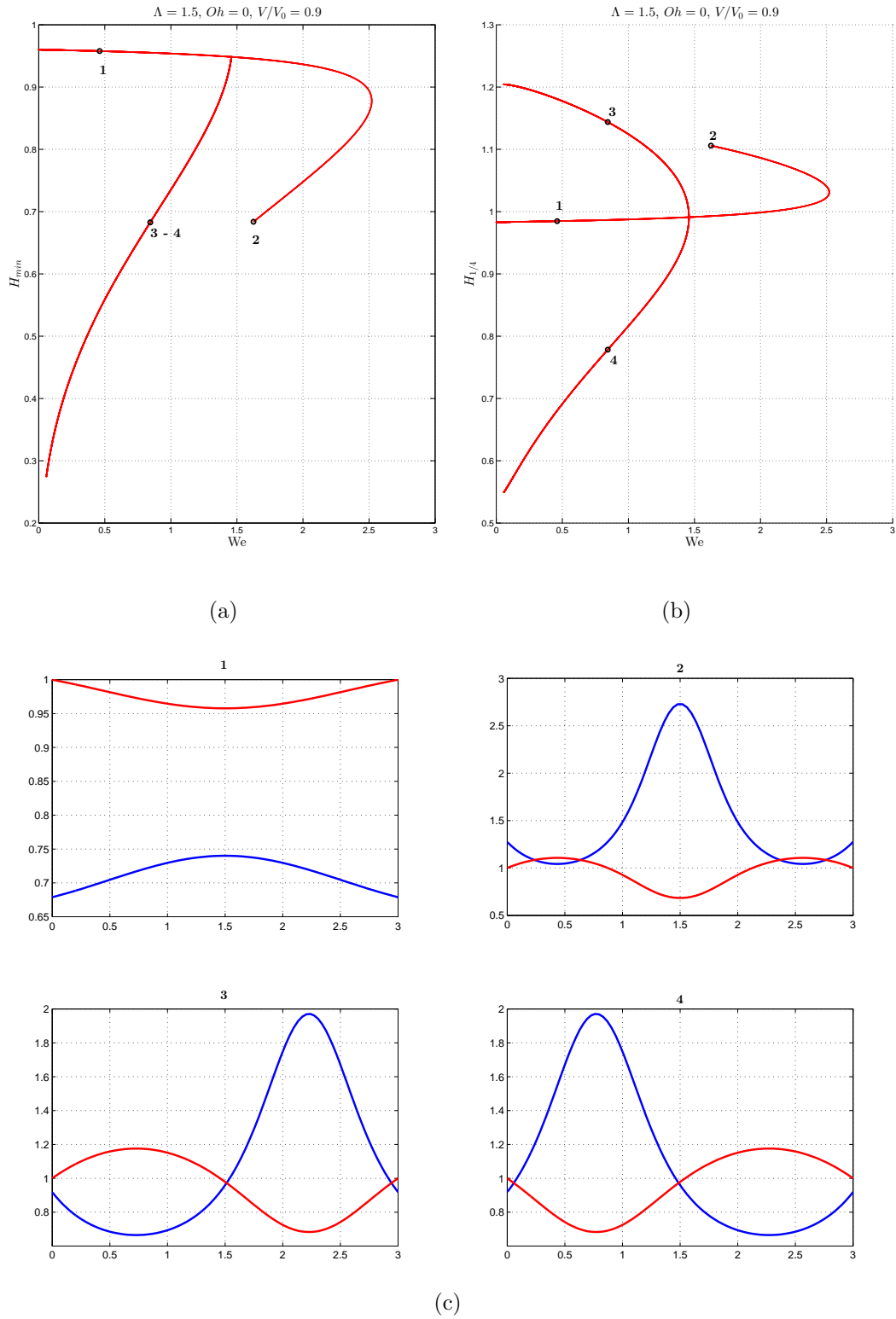


Figure 6.5: Examples of interface shapes (c) of bifurcation diagram (a) and (b) (red lines are interfaces, blue lines are the velocity profile)

curve in We-minimum radius coordinate is presented.

The main change is the appearance for $Oh \neq 0$ of two different paths for the asymmetric shape of interface, one for the backward and one for the forward, while for $Oh = 0$ they collide in only one path. Another important change in the first branch due to the viscosity is the decrease of stability limit at lower Weber number as the viscosity increase.

Indeed, viscosity is responsible for the disappearance of the second branch and for changing its stability. As we can see in figure 6.6, the second branch disappear for viscosity greater than $Oh \gtrsim 2.95 \times 10^{-2}$, while for viscosity larger than $Oh \gtrsim 1.5 \times 10^{-2}$ the Hopf bifurcation is no longer available.

6.3 Comparison with quasi-static simulations

The bifurcation diagram obtained from these equations in the case of $\Lambda = 1$ is compared with quasi-static result of time-integration algorithm based on Eggers equation (2.6) and with axisymmetric simulations with the GERRIS Flow Solver (see figure 6.7, 6.8, 6.9). Results show a good agreement, especially for ratios of volume $V < 0.9$. The comparison is less satisfactory for V close to 1, especially during the swing phase of the interface (the red area just before the breakage in figure 6.9).

While for $V \lesssim 0.85$ the one-dimensional model appears to predict with great accuracy the breaking point, for greater volumes the occurrence of nonlinear effect (oscillation) limits the use of this simplified model (see figure 6.7). In support of this, dynamical simulations based on one-dimensional model can not "jump" the second branch of solution and go straight to the breakage (see figure 6.8 and 6.9).

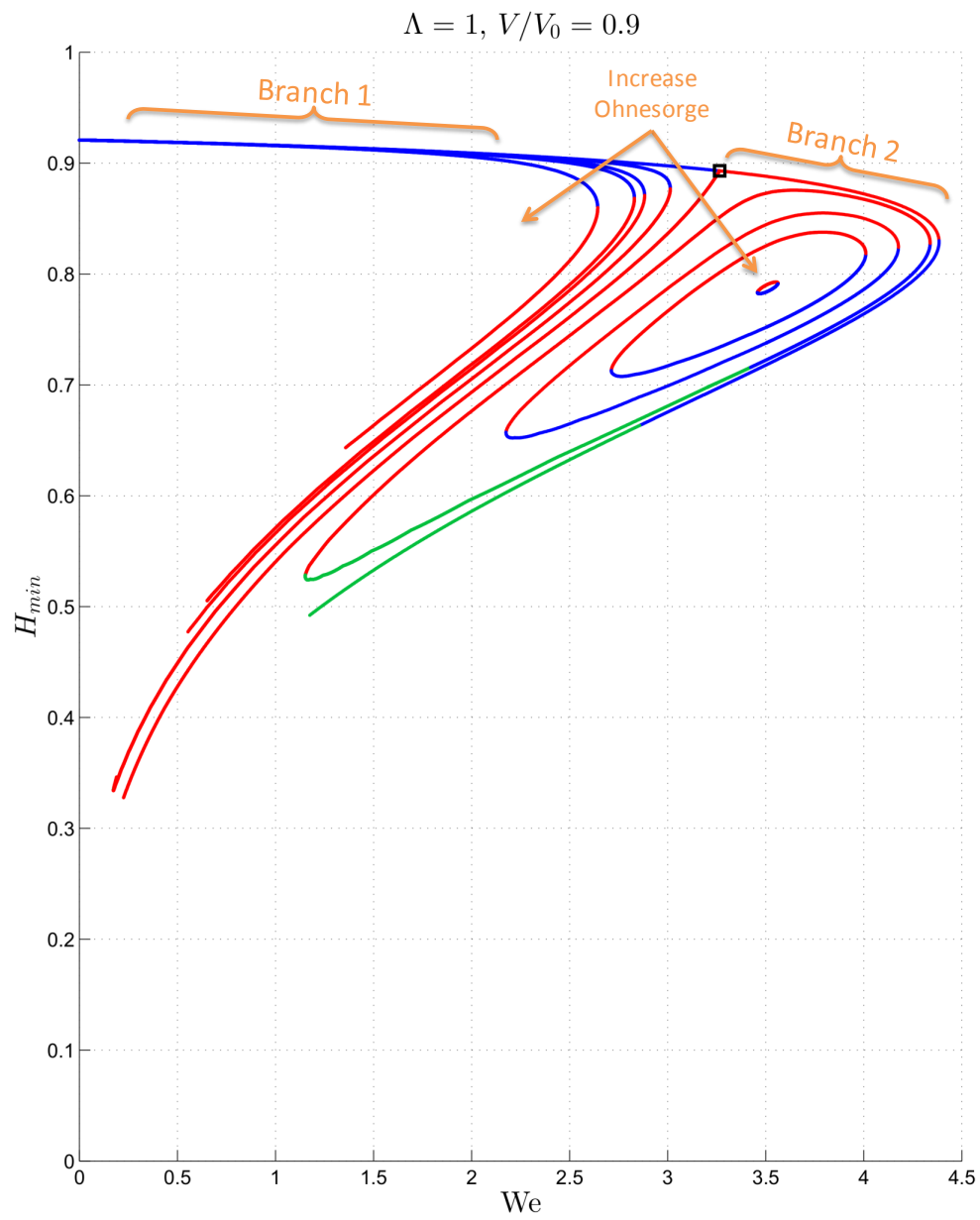


Figure 6.6: Influence of Ohnesorge number on bifurcation diagram

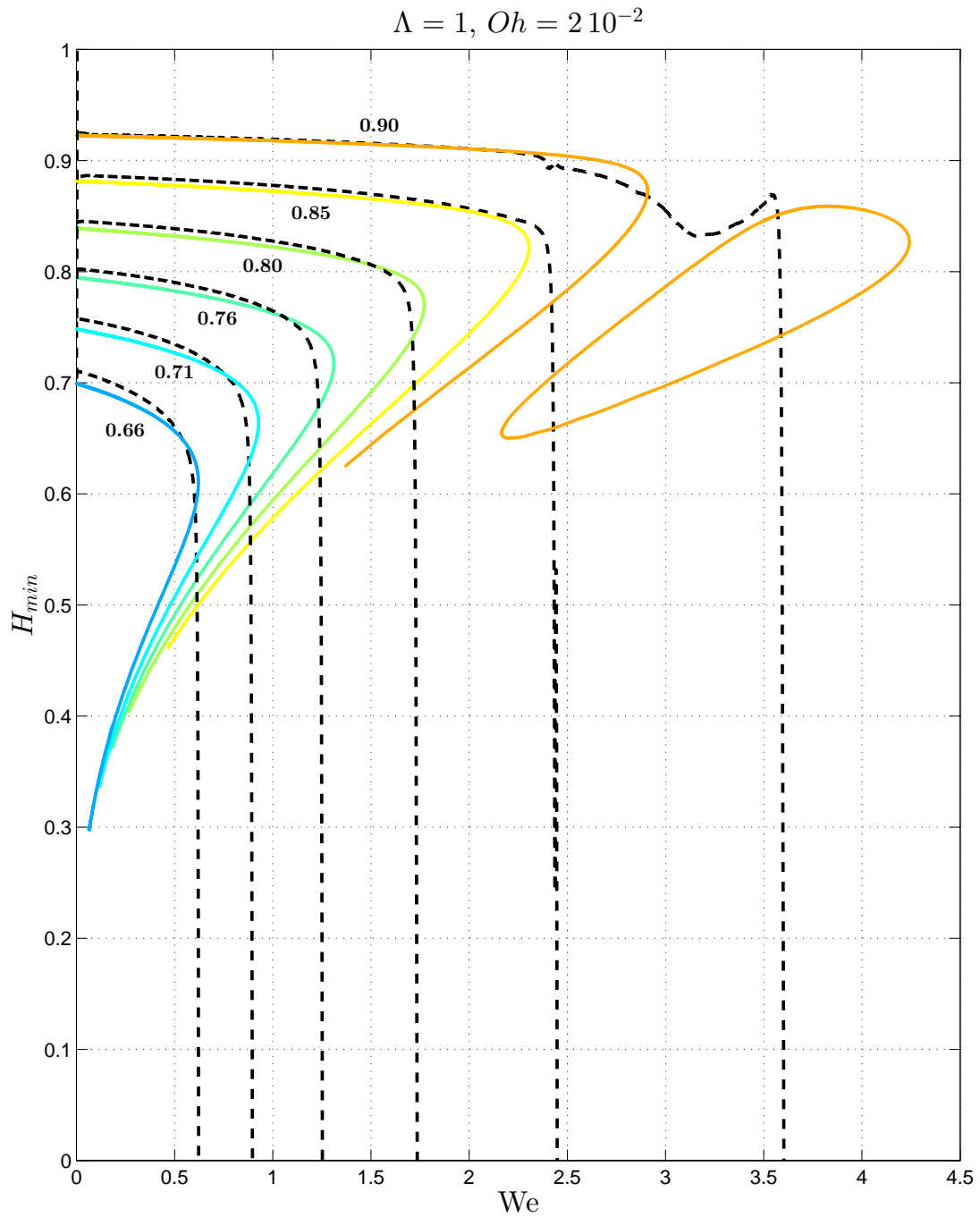


Figure 6.7: Comparison between equilibrium points (solid line) and quasi-static axisymmetric simulations on GERRIS (dashed line). Numbers on the curve indicate the value of volume

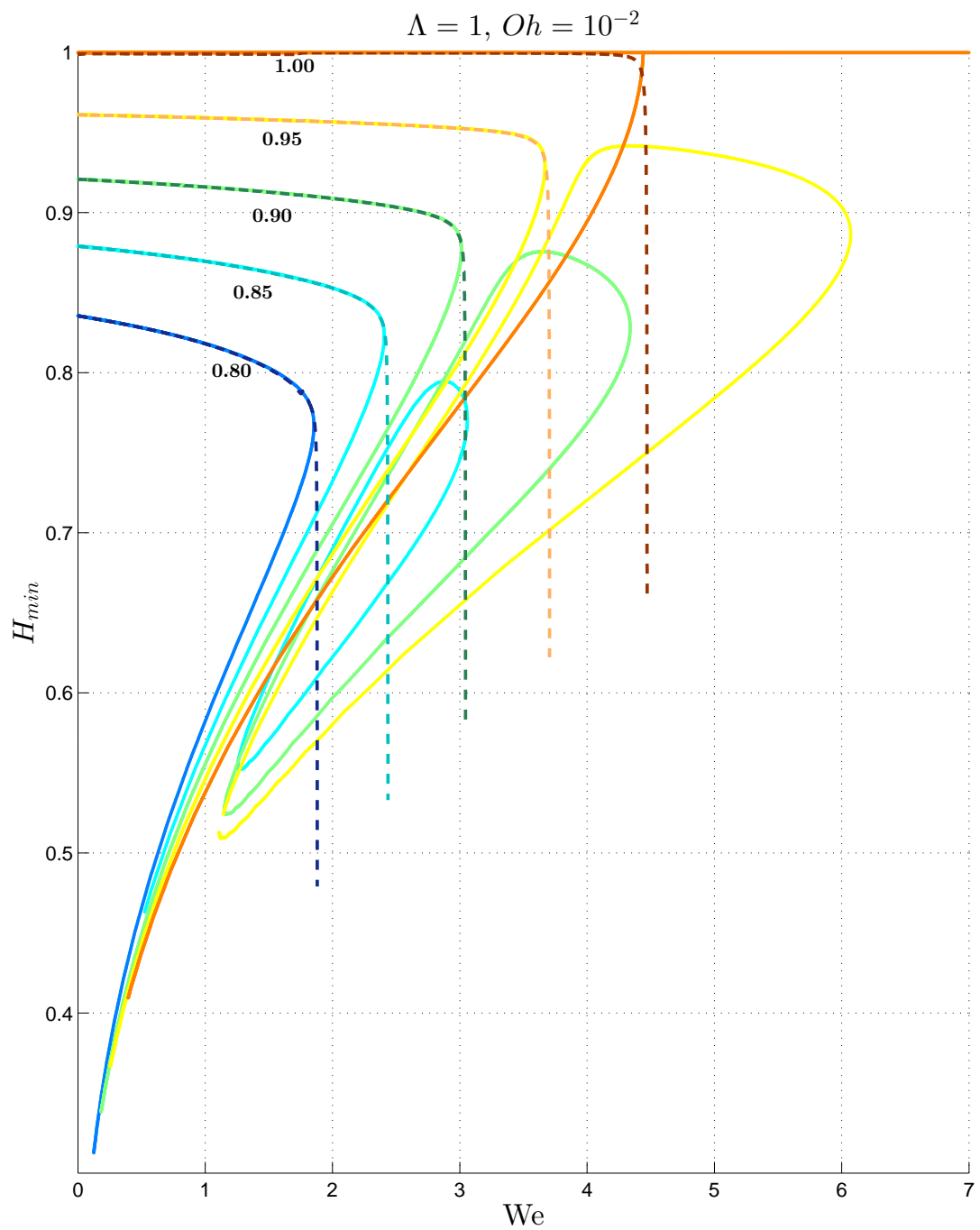


Figure 6.8: Comparison between equilibrium points (solid line) and quasi-static time-integration of the model equations (dashed line). Numbers on the curve indicate the value of volume

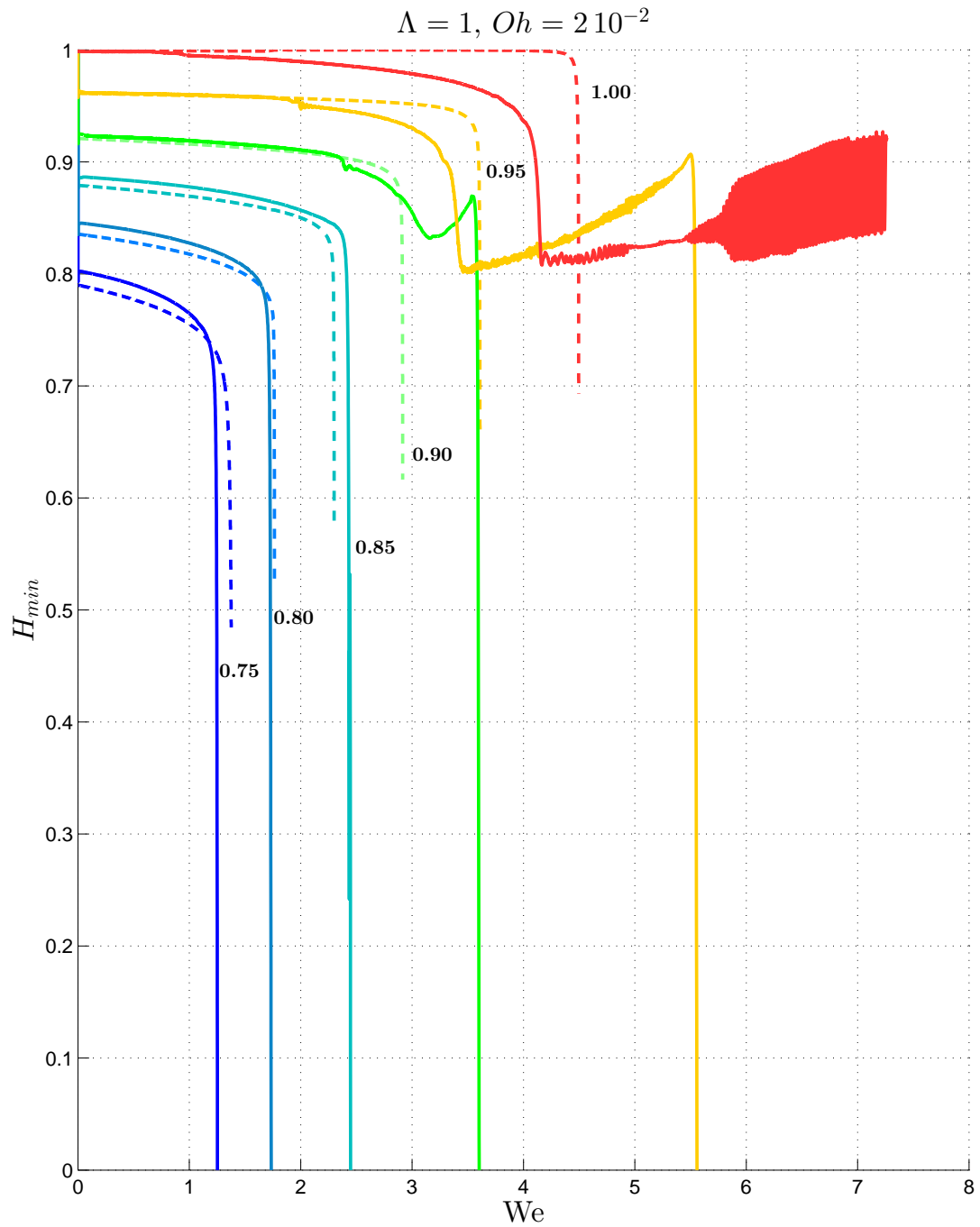


Figure 6.9: Comparison between time-integration of the model equations (dashed line) and axisymmetric GERRIS simulations (solid line). Numbers on the curve indicate the value of volume

7 Conclusions and future work

The main objective of this thesis was to develop a tool to study the stability of liquid bridges to better understand the complex phenomenon of drop formation and the peculiar effect of "escape" from breakup [11]. This aim has been reached developing a MATLAB code capable of numerically solving the fluid flow based on Eggers and Dupont one-dimensional model, supported by the implementation of a method for continuation of solution, bifurcation point detection and branch switching. Furthermore, a time-integration algorithm has been developed to compare solutions of the one-dimensional model with dynamical solutions.

Therefore, the stability of the capillary bridge has been numerically investigated in two different ways, the static and quasi-static case. The results obtained are in good agreement with the theoretical results in the literature.

In addition, the comparison with axisymmetry GERRIS simulations in the $\Lambda = 1$ case shows a very good agreement for the first branch but a limit in describing the "jump" to slapping state. For $V \lesssim 0.85$, the neck of the bridge, initially in the middle of the capillary bridge, decreases progressively and moves downstream of the system (in the same direction as the velocity), then tends to break. If the aspect ratio of the bridge is quite large ($\Lambda \approx 3$), the bridge will come close to Rayleigh-Plateau instability and thus the neck stay in the middle of the system and tends to break at zero Weber number. In this case, the one-dimensional model predicts with good accuracy the break point. For $V \gtrsim 0.85$, more complex behaviour occurs, including nonlinear oscillations. The dynamic simulations suggest the presence of a second unstable branch of solutions which can not be predicted with accuracy with the use of the one-dimensional model.

There are various developments of this work which are worth to be carried out. Among them, further examination on the influence of parameters on the second branch which is the possible key to understand the "escape" phenomenon. In addition, a two-dimensional model can be developed to achieve better results for the slapping zone, to include all phenomena that a one-dimensional model may not be able to capture.

Acknowledgements/Ringraziamenti

I would like to really thank Prof. Alessandro Bottaro and Dott. Jerome Hoepffner for having proposed to me this interesting and prolific topic, and for the opportunity to work on it at UPMC in Paris. I am thankful to Dott. Hoepffner for the way he welcomed me in his team, for all the time he dedicate to me in this interesting experience. I am very grateful to Prof. Bottaro for this opportunity and especially for his patience and trust. I also want to express gratitude to Gounseti Paré, excellent research partner who guided me in this five month.

I want to express thankfulness to al the UPMC staff for welcoming me as a little brother, for their friendship and support. A special thanks goes to Luca, Marcello, Valentina and Simonà for their continuous help and for every weekend together.

I hope nobody will feel offended if I switch from English to Italian to thank all the people that have been close to me in the last five years, of which this thesis and my graduation are somehow a conclusion.

Vorrei ringraziare innanzitutto i miei genitori, per tutto il supporto e la fiducia datami in questi anni di studio, perchè è principalmente grazie a loro se sono riuscito a raggiungere questo traguardo.

Ringraziamento di cuore la mia ragazza Camilla, che ha condiviso con me questo lungo cammino stringendomi per mano nei momenti difficili ed gioendo con me nei successi, che nonostante i miei difetti ha la pazienza di rimanere ancora al mio fianco e illuminare ogni mio giorno con la sua unicità.

Un ringraziamento particolare va a Federica, compagna di risate e felicit, la migliore amica che si potrebbe incontrare, e a Carlo, ormai come un fratello, compagno di sempre, che neanche la distanza ha potuto allontanare.

Infine, ma non per importanza, vorrei ringraziare coloro i quali hanno condiviso con me questi anni di corsi ed esami e tutte le altre persone fanno parte della mia vita che non ho lo spazio per citare uno ad uno, ma sanno di meritare un grazie gigante.

References

- [1] Gerris flow solver. www.gfs.sourceforge.net.
- [2] L. V. Barmin, B. E. Vershinin, I. G. Levitina, and A. S. Senchenkov. Stability of liquid rotating zone. *Izv. Akad. Nauk SSR Ser. Fiz.*, 49:661, 1985.
- [3] D. B. Bogy. Drop formation in a circular liquid jet. *A. Rev. Fluid Mech.*, 11:207–228, 1979.
- [4] P. S. de Laplace. *Mécanique Céleste*. Courier, Paris, 1805. Supplement au X Livre.
- [5] E. Doedel, H. B. Keller, and J. P. Kernevez. Numerical analysis and control of bifurcation problems: (i) bifurcation in finite dimensions. *Int. J. Bifurcation and Chaos*, 1(3):493–520, 1991.
- [6] J. Eggers. Nonlinear dynamics and breakup of free-surface flows. *Review of Modern Physics*, 69(3):865–929, 1997.
- [7] J. Eggers. A brief history of drop formation. In P. Alart, O. Maisonneuve, and R. Rockafellar, editors, *Nonsmooth Mechanics and Analysis*, volume 12 of *Advances in Mechanics and Mathematics*, pages 163–172. Springer US, 2006.
- [8] J. Eggers and T. F. Dupont. Drop formation in a one-dimensional approximation of the Navier-Stokes equation. *J. Fluid Mech.*, 262:205–221, 1994.
- [9] J. Eggers and E. Villermaux. Physics of liquid jets. *Rep. Prog. Phys.*, 71:1–79, 2008.
- [10] R. Gillette and R. Dayson. Stability of fluid interfaces of revolution between equal solid circular plates. *Chem. Eng. J.*, 2:44–54, 1971.
- [11] J. Hoepffner and G. Paré. Recoil of a liquid filament: escape from pinch-off through creation of a vortex. *J. Fluid Mech.*, 734:183–197, 2013.

- [12] H. B. Keller. *Applications of Bifurcation Theory*, chapter Numerical solution of bifurcation and nonlinear eigenvalue problems, pages 359–284. Academic Press, 1977.
- [13] H. C. Lee. Drop formation in a liquid jet. *IBM J. Res. Dev.*, 18:364–369, 1974.
- [14] P. Lenard. *Ann. Phys. Chem.*, 30:209, 1887.
- [15] B. J. Lowry and P. H. Steen. Capillary surfaces: stability from families of equilibria with application to the liquid bridge. *Proceedings: Mathematical and Physical Sciences*, 449:441–439, 1995.
- [16] J. Maddocks. Stability and folds. *Arch. Rational Mech. Anal.*, 99(4):301–328, 1987.
- [17] I. Martinez. Stability of axisymmetric liquid bridges. In *ESA SP-191*, page 267. European Space Agency, Paris, 1983.
- [18] I. Martinez and J. M. Perales. Mechanical behaviour of liquid bridges in microgravity. In R. Monti, editor, *Physics of Fluids in Microgravity*, pages 21–45. Taylor & Francis, 2001.
- [19] J. Meseguer, L. A. Slobozhanin, and J. M. Perales. A review on the stability of liquid bridges. *Adv. Space Res.*, 16:5–14, 1995.
- [20] J. Plateau. *Acad. Sci. Bruxelles Mm.*, 16:3, 1843.
- [21] J. Plateau. *Acad. Sci. Bruxelles Mm.*, 23:5, 1849.
- [22] L. Rayleigh. *Proc. London Math. Soc.*, 10:4, 1879. appeared in the vol. of 1878.
- [23] A. Sanz and I. Martinez. Minimum volume for a liquid bridge between equal disks. *J. Colloid Interface Sci.*, 93:235, 1983.
- [24] F. Savart. *Ann. Chim.*, 53:337, 1833. plates in vol. 54.

- [25] L. A. Slobozhanin. Problems on the stability of liquids in equilibrium, appearing in spatial technology. In *Hydromechanics and Heat and Mass Transfer in Zero-Gravity*, page 9. Nauka, Moscow, 1982.
- [26] L. A. Slobozhanin. Some problems of equilibrium stability of zero-g liquid bridges. In *Hydromechanics and Heat/Mass Transfer in Micro-gravity*, page 185. Gordon and Bleach, Philadelphia, 1992.
- [27] L. A. Slobozhanin, J. I. D. Alexander, and V. D. Patel. The stability margin for stable weightless liquid bridges. *Phys. Fluids*, 14:209–224, 2002.
- [28] J. A. Weideman and S. C. Reddy. A matlab differentiation matrix suite. *ACM Trans. Math. Softw.*, 26(4):465–519, 2000.
- [29] T. Young. *Philos. TRans. R. Soc. London*, 95:65–87, 1804.